Barbara Süsser-Rechberger, BSc

New Results on Symbol Rate Estimation in Digital Satellite Receivers

MASTER'S THESIS

to achieve the university degree of

Diplom-Ingenieurin

Master's degree programme: Space Sciences and Earth from Space

submitted to

Graz University of Technology

Supervisor

Assoc.Prof. Dipl.-Ing. Dr.techn. Wilfried Gappmair

Institute of Communication Networks and Satellite Communications

Graz, April 2018

AFFIDAVIT

I declare that I have authored this thesis independently, that I have not used other than the declared sources/resources, and that I have explicitly indicated all material which has been quoted either literally or by content from the sources used. The text document uploaded to TUGRAZonline is identical to the present master's thesis.

Date

Signature

Danksagung

Diese Diplomarbeit widme ich meinem Papa und meiner Mutti, die immer an mich geglaubt und ermutigt haben. Meinen Geschwistern Marion, Elisabeth und Johanna, meinen Neffen Raphael und Jonathan, sowie Andreas, Thomas und Mirnesa danke ich, dass sie mich immer ermuntert haben und immer für mich da waren. Meinem Mann Andreas danke ich für die jahrelange liebevolle Unterstützung und auch für die vielen fachlichen Diskussionen.

An dieser Stelle ein großes Dankeschön an meinen Betreuer Assoc.Prof. Dr. Wilfried Gappmair, der mich immer unterstützt, gefördert und gefordert hat.

Des Weiteren danke ich meinem unmittelbaren Vorgesetzten Dipl.-Ing. Helmut Paulitsch, mit dessen Verständnis Beruf und Studium leichter zu vereinbaren waren.

Zu guter Letzt möchte ich mich auch bei allen anderen bedanken, die mich bei der Durchführung dieser Diplomarbeit unterstützt haben.

Graz, im April 2018 Barbara Süsser-Rechberger

Kurzfassung

Die Schätzung der Symbolrate bzw. der Symbolperiode ist von großer Bedeutung, wenn sehr lange Datenpakete bei der Satellitenkommunikation verwendet werden. Abweichungen der Symbolrate führen zu einer nicht korrekten Abtastung und zu einem Verlust von mehreren Symbolen pro Datenpaket, welche auch durch eine Fehlerkorrektur nicht wiederherstellbar sind.

In dieser Masterarbeit werden vier verschiedene Methoden zur Schätzung der Symbolrate bzw. Symbolperiode untersucht und miteinander verglichen. Die erste Methode verwendet einen datenunterstützten Algorithmus, welcher in Form einer Korrelationsfilterbank implementiert ist. Der zweite Algorithmus ist ebenfalls datenunterstützt und schätzt die Symbolrate anhand des Symbol Timings von zwei Pilotsequenzen. Bei der dritten Methode wird ein auf der Kombination von datenunterstützt/nicht datenunterstützt beruhender Algorithmus verwendet, der auch auf der Timing-Schätzung basiert. Die vierte Variante ist eine rein nicht datenunterstützte Methode und als Regelschleife implementiert.

Die Analyse zeigt, dass die verschiedenen Varianten zuverlässige Ergebnisse liefern, welche jedoch auch abhängig von bestimmten Parameter sind, wie zum Beispiel der Auflösung zwischen den Filterbankelementen, dem Roll-off Faktor der im Sender und Empfänger verwendeten pulsformenden Filter, der Länge der Pilotsequenz oder auch der Bandbreite der Regelschleife.

Abstract

The estimation of symbol rate or symbol period is of paramount importance, if very long data packets are used in satellite communications. Deviations of the symbol rate lead to an incorrect sampling and loss of several symbols per data package, which can not be recovered by an error correction.

In this master thesis, four different methods for symbol rate estimation are investigated and compared. The first method uses a data-aided algorithm, which is implemented in the form of a correlation filter bank. The second algorithm is also a data-aided one and estimates the symbol rate based on the symbol timing of two pilot sequences. The third method uses a hybrid data-aided/non-data-aided algorithm with rate estimates also based on the timing estimation. The fourth variant is a purely non-data-aided method implemented as a control loop.

The analysis shows that the different variants provide reliable results, which depend on certain parameters, such as the resolution between the correlation filter bank elements, the roll-off factor of the pulse shaping filter in the transmitter and receiver, the length of the pilot sequence or also the bandwidth of the control loop.

Contents

Acronyms

APSK amplitude phase shift keying.

AWGN additive white Gaussian noise.

BPSK binary phase shift keying.

CRLB Cramer-Rao lower bound.

DA data-aided.

DFT discrete Fourier transformation.

DMF derivative matched filter.

DVB digital video broadcasting.

FB feedback.

FF feedforward.

FIM Fisher information matrix.

ISI inter-symbol interference.

L&R Luise-Reggiannini.

LLF log-likelihood function.

MCRLB modified Cramer-Rao lower bound.

MEV mean estimator value.

MF matched filter.

ML maximum-likelihood.

NDA non-data-aided.

O&M Oerder-Meyr.

OSR oversampling rate.

PLL phased-locked loop.

PPM parts per million.

PRN pseudo-random number.

PSK phase shift keying.

QPSK quadrature phase shift keying.

RCos raised cosine.

RRCos root-raised cosine.

SNR signal-to-noise ratio.

TED timing error detector.

1 Introduction

In satellite communication networks a reliable reception of data is only possible if the appropriate demodulator has knowledge about the relevant transmission parameters or if these parameters are estimated by suitably designed algorithms. This process is known as parameter estimation and synchronisation [1], and is done via feedforward (FF) or feedback (FB) schemes. It has to be considered that synchronisation of transmission parameters is a multi-dimensional, non-linear and stochastic optimization problem. The transmission parameters include the optimum sampling instant τ, the symbol period T or symbol rate $1/T$, the carrier frequency offset F, the carrier phase θ and the signal amplitude A.

This work investigates the symbol rate estimation, which is of great importance especially for very long data packets which are used in the new standard for digital video broadcasting via satellite (DVB-S2x) [2]. For such long data frames, a symbol rate deviation in the parts per million (PPM) range leads to non-correct sampling and symbol loss. The mismatch of the oscillators in sender and receiver as well contribute to this context. In practice, the oscillators have a deviation in the lower PPM range. In this master thesis, four different methods for symbol rate estimation are analysed with respect to their robustness and accuracy.

2 Signal Model

This chapter describes the baseband model [1] used for analysis and simulation. It is assumed that the data symbols $c_i = a_i + jb_i$ are zero mean and normalised to unit variance. The data symbols are independent and identically distributed and belong to an M-ary alphabet C which is either a phase shift keying (PSK) or an amplitude phase shift keying (APSK) modulation scheme. For example, in the DVB-S2x standard [2], 16/32-APSK schemes are defined. The baseband pulse $h(t)$ has a root-raised cosine (RRCos) shape with a roll-off factor α, where $0 \leq \alpha \leq 1$.

The transmitter signal can be expressed by

$$s(t) = \sum_i c_i h(t - iT) \tag{2.1}$$

where T denotes the symbol period. The signal $s(t)$ is amplified by a real-valued gain factor $A > 0$ and is rotated by the carrier phase $\theta \in [-\pi, \pi)$.

Additionally, for the signal model following impairments have to be considered:

- Symbol timing τ: Due to propagation and transponder delay, a symbol timing has to be taken into account.
- Carrier frequency offset F: This impairment is caused by the Doppler effect and by the fact that there is an oscillator mismatch between sender and receiver.
- Additive white Gaussian noise (AWGN) $w(t)$: Thermal noise which is produced in any receiver.

Therefore, the received signal is given by

$$r(t) = Ae^{j(2\pi Ft+\theta)}s(t - \tau) + w(t) \tag{2.2}$$

where $w(t)$ is a complex-valued AWGN process with variance $\sigma_w^2 = N_0/2$ for both real and imaginary part. Thus, with $E_s = A^2$, the signal-to-noise ratio (SNR) per symbol is formulated as

$$\gamma_s = E_s/N_0 = \frac{A^2}{2\sigma_w^2} \tag{2.3}$$

The complete baseband model for symbol rate estimation is shown by the block diagram in Figure 2.1.

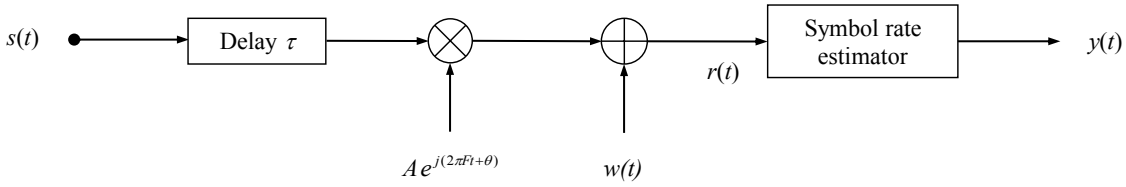

Figure 2.1: Baseband model for symbol rate estimation

3 Joint Data-Aided Parameter Estimation

3.1 Modified Cramer-Rao Lower Bound and Jitter Variance

For any estimation or synchronisation algorithm, the jitter variance is a most important figure of merit. The theoretical limit of the jitter variance is given by the Cramer-Rao lower bound (CRLB).

As described in [1], the CRLB of a transmission parameter u_i is determined by,

$$\mathrm{CRLB}(u_i) = [\mathbf{J}^{-1}(\mathbf{u})]_i \tag{3.1}$$

where $[\cdot]_i$ indicates the (i)-th diagonal element of the inverted Fisher information matrix (FIM) $\mathbf{J}(\mathbf{u})$. The vector $\mathbf{u}$ denotes the set of transmission parameters including the signal amplitude A, the carrier phase θ, the carrier frequency offset F, the symbol timing τ and the symbol period T. The FIM element for row i and column k is determined by

$$[\mathbf{J}(\mathbf{u})]_{i,k} = -\mathbb{E}\left[\frac{\partial^2}{\partial u_i \partial u_k}\Lambda(\mathbf{r};\mathbf{u})\right] \tag{3.2}$$

where $\mathbf{r}$ is the vector representation of (2.2) and $\Lambda(\cdot)$ is the log-likelihood function (LLF) describing the L observables in $\mathbf{r}$. The expectation $\mathbb{E}[\cdot]$ is related to the AWGN process. Due to the fact that the modified Cramer-Rao lower bound (MCRLB) is much easier from the analytical point of view, it is commonly used in practice [3].

The relationship between the true CRLB and the MCRLB is described in [4], where it is shown that $\mathrm{MCRLB}(u_i) \leq \mathrm{CRLB}(u_i)$. For determining the MCRLB, the analytical background denoted in (3.1) and (3.2) can be applied too, but it has to considered that the expectation $\mathbb{E}[\cdot]$ relates now to data and noise.

The mathematical derivation of the modified FIM entries leads to the following formulas for the diagonal elements [5]:

$$J_{1,1} = \frac{2L\gamma_s}{A^2} \tag{3.3}$$

$$J_{2,2} = 2L\gamma_s \tag{3.4}$$

$$J_{3,3} = \frac{2\pi^2 T^2 L(L^2-1)\gamma_s}{3} \tag{3.5}$$

$$J_{4,4} = -2L\gamma_s \ddot{g}(0) \tag{3.6}$$

$$J_{5,5} = -\frac{2\gamma_s L(L^2-1)\ddot{g}(0)}{12} \tag{3.7}$$

The off-diagonal FIM elements are all zero. Note that $\ddot{g}(0)$ in (3.6) is the second-order derivative of the raised cosine (RCos) function $g(t)$ evaluated at $t = 0$; $\ddot{g}(0)$ normalized to the squared symbol period results in $-T^2\ddot{g}(0) = \frac{1}{3}\pi^2(1+3\alpha^2) - 8\alpha^2$. It is to be mentioned that the MCRLBs for signal amplitude, carrier frequency offset and symbol timing are mostly represented in normalized form:

$$\mathrm{MCRLB}(a) = \frac{\mathrm{MCRLB}(A)}{A^2} = \frac{1}{A^2 J_{1,1}} = \frac{1}{2L\gamma_s} \tag{3.8}$$

$$\mathrm{MCRLB}(\theta) = \frac{1}{J_{2,2}} = \frac{1}{2L\gamma_s} \tag{3.9}$$

$$\mathrm{MCRLB}(\nu) = \mathrm{MCRLB}(FT) = \frac{T^2}{J_{3,3}} = \frac{3}{2\pi^2 L(L^2-1)\gamma_s} \tag{3.10}$$

$$\mathrm{MCRLB}(\epsilon) = \frac{\mathrm{MCRLB}(\tau)}{T^2} = \frac{1}{T^2 J_{4,4}} = -\frac{1}{2L\gamma_s T^2 \ddot{g}(0)} \tag{3.11}$$

$$\mathrm{MCRLB}(\eta) = \frac{\mathrm{MCRLB}(T)}{T^2} = \frac{1}{T^2 J_{5,5}} = -\frac{12}{2L(L^2-1)\gamma_s T^2 \ddot{g}(0)} \tag{3.12}$$

Note that in (3.10) the carrier frequency offset is normalized to the symbol period T, which is denoted by $\nu = FT$.

3.2 Simplified Approach Compared with Maximum-Likelihood Solution

For estimation purposes, either the Euclidean distance or the correlation between a test function and the received signal can be used. The Euclidean metric is optimal in the maximum-likelihood

(ML) sense, if the noise follows a Gaussian distribution. Thus, successful estimation is indicated through a minimum Euclidean distance or a maximum correlation output for a specific value of the transmission parameter vector. As described in [1], the ML solution can be written as

$$\hat{\mathbf{u}} = \arg\max_{\tilde{\mathbf{u}}} \Lambda(\mathbf{r}; \tilde{\mathbf{u}}) \tag{3.13}$$

where $\tilde{\mathbf{u}}$ is the parameter vector, which maximises the LLF. The maximum-likelihood estimation can be done via the Newton-Raphson method [6]. This algorithm uses an iterative procedure to approach the maximum of a log-likelihood function and is given by

$$\tilde{\mathbf{u}}^{(n)} = \tilde{\mathbf{u}}^{(n-1)} - \mathbf{T}^{-1} \cdot \mathbf{t} \,|_{\mathbf{u}=\tilde{\mathbf{u}}^{(n-1)}}, \quad n = 1, \ldots, n_{max} \tag{3.14}$$

where $[\mathbf{T}]_{i,k}$ denotes the Jacoby matrix and is computed as follows:

$$t_i = \frac{\partial \Lambda(\mathbf{r}; \mathbf{u})}{\partial u_i}, \quad T_{i,k} = [\mathbf{T}]_{i,k} = \frac{\partial t_i}{\partial u_k} \tag{3.15}$$

Due to the iterative concept, an initial value $\tilde{\mathbf{u}}^{(0)}$ is needed.

However, this method is problematic in terms of convergence and stability. Also, the start value has to be chosen suitably. Therefore, a simplified approach is investigated in the sequel.

3.2.1 Joint Symbol Rate and Timing Recovery

Generally, the symbol period, respectively the symbol rate, differs between sender and receiver. Mismatching oscillators in the receiver and transmitter contribute to this deviation. The correlation suffers from such deviation in the way that a reduced correlation peak is delivered. In order to estimate the symbol period mismatch, a bank of correlation filters is used, each of which configured with different symbol periods, described by $T_m = T_0 + m\Delta T$, where $m \in \mathbb{Z}$ is the index of the filter elements, T_0 is the nominal/reference period, and ΔT is the resolution step between them. It is assumed that the correlation filter which uses the same symbol rate as the transmitter RRCos filter has the index 0. Positive indices indicate an increasing symbol period, negative indices indicate a decreasing symbol period. It is obvious that an equal spacing between the filter elements can be reached. The correlation filter bank model is shown in Figure 3.1.

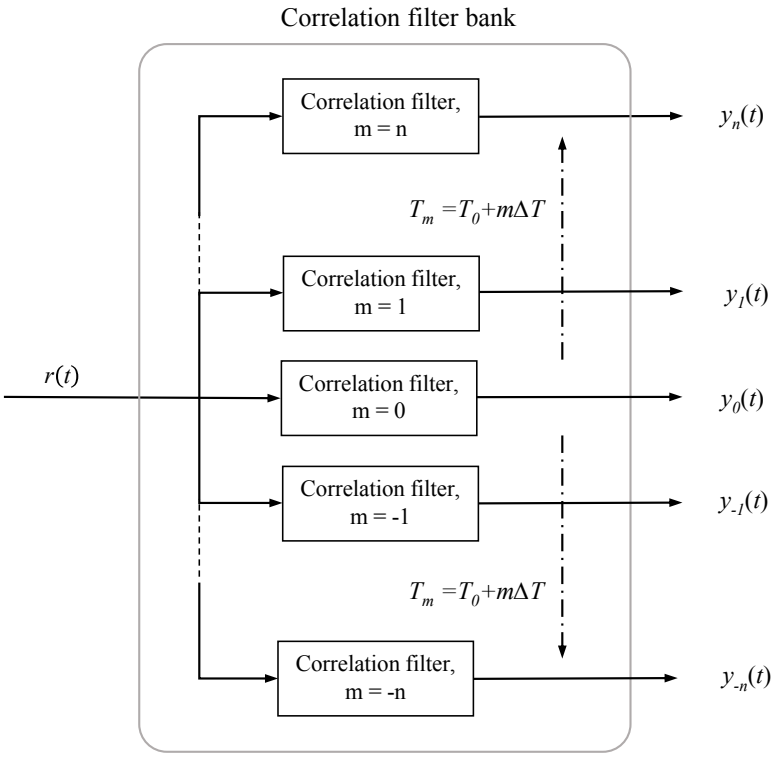

Figure 3.1: Correlation filter bank

The simplified approach assumes that there exists no carrier frequency offset and the carrier phase is averaged out. Also, one has to take into account that for timing and rate estimation the amplitude A is not relevant, so this is only a two-dimensional optimisation problem. Therefore, the simplified log-likelihood function Λ' can be expressed by

$$\Lambda'(\mathbf{r};\mathbf{u}) \sim \left| \sum_{k=-(L-1)/2}^{(L-1)/2} \omega_k^* x_k \right| \tag{3.16}$$

where ω_k denotes the pilot sequence or preamble and x_k are the samples at the correlation filter output. The joint estimation of τ and T is then achieved by

$$(\hat{\tau}, \hat{T}) = \arg\max_{\tilde{\tau},\tilde{T}} \Lambda'(\mathbf{r};\tilde{\tau},\tilde{T}) = \arg\max_{\tilde{\tau},\tilde{T}} \left| \int_{-\infty}^{\infty} \Omega(t,\tilde{T}) r(t+\tilde{\tau}) dt \right| \tag{3.17}$$

In (3.17) it is obvious that the received signal is folded with the correlation filter function $\Omega(t, \tilde{T})$. The correlation filter function describes the weighting of the pilot sequence with the impulse response function of a RRCos filter and is given by

$$\Omega(t, \tilde{T}) = \sum_{k=-(L-1)/2}^{(L-1)/2} \omega_k^* h(t - k\tilde{T}) \tag{3.18}$$

After some algebra it can be shown that

$$\sum_{k=-(L-1)/2}^{(L-1)/2} \omega_k^* x_k = \int_{-\infty}^{\infty} \Omega(t, \tilde{T}) r(t + \tilde{\tau}) dt \tag{3.19}$$

The discretisation of the optimization problem, assuming a sampling period $T_s = T_0/N_s$, determined by the oversampling factor N_s, can be described as follows:

$$Y_{m,\mu} = \left| \sum_{i \in \mathcal{I}} \Omega(iT_s, T_m) r[(i + \mu)T_s] \right| \tag{3.20}$$

where μ is the timing offset between receiver signal and pilot sequence and m is the index of the correlation filter bank. Due to avoiding the aliasing effect, $N_s \geq 2$ is necessary. Hence, all elements in the correlation filter bank with mismatching symbol period deliver a degraded correlation result. The closer the symbol rate of the filter matches the symbol rate of the received signal, the higher the correlation peak becomes. Therefore, choosing the filter with the maximum correlation result gives the estimate for the filter index $\hat{m}$ and the timing offset $\hat{\mu}$:

$$(\hat{m}, \hat{\mu}) = \arg \max_{m,\mu} Y_{m,\mu} \tag{3.21}$$

As described in [7], the symbol timing is estimated via a parabolic interpolation of the main lobe, given by

$$\hat{\tau} = \left(\hat{\mu} - \frac{1}{2} \frac{Y_{\hat{m},\hat{\mu}+1} - Y_{\hat{m},\hat{\mu}-1}}{Y_{\hat{m},\hat{\mu}+1} - 2Y_{\hat{m},\hat{\mu}} + Y_{\hat{m},\hat{\mu}-1}} \right) T_s \tag{3.22}$$

Just like the estimation of symbol timing, the symbol period estimation is also done with a

parabolic interpolation:

$$\hat{T} = T_0 + \left(\hat{m} - \frac{1}{2} \frac{Y_{\hat{m}+1,\hat{\mu}} - Y_{\hat{m}-1,\hat{\mu}}}{Y_{\hat{m}+1,\hat{\mu}} - 2Y_{\hat{m},\hat{\mu}} + Y_{\hat{m}-1,\hat{\mu}}} \right) \Delta T \tag{3.23}$$

Referring to [7], the performance degradation caused by a non-negligible frequency offset can be mitigated by dividing the observation window into K smaller and non-overlapping parts $\mathcal{I}_k$, where $\mathcal{I} = \bigcup_{k=1}^{K} \mathcal{I}_k$. Corresponding to the partitioning the following modified correlation process delivers the final result [8]:

$$Y_{m,\mu} = \sum_{k=1}^{K} \left| \sum_{i \in \mathcal{I}_k} \Omega(iT_s, T_m) r[(i+\mu)T_s] \right| \tag{3.24}$$

3.2.2 Carrier Frequency Recovery

The carrier frequency offset reduces the signal power at the filter output and violates the Nyquist criterion. After successful synchronisation and to ensure that the recovery of the carrier phase is reliable, the carrier frequency offset has to be estimated by some powerful FF algorithm. In this work, the Luise-Reggiannini (L&R) algorithm [9] is used. By means of the correlation result

$$R_n = \frac{1}{L-n} \sum_{k=n}^{L-1} \hat{z}_k \hat{z}_{k-n}^* \tag{3.25}$$

the residual frequency estimate is computed as follows:

$$\hat{\nu} = \frac{1}{\pi(K+1)} \arg\left(\sum_{n=1}^{K} R_n \right), \quad 1 \leq K < L \tag{3.26}$$

where $\nu = FT$ is the normalized frequency offset and K is a form factor.

The term $\hat{z}_k = \omega_k \hat{y}_k$ describes the multiplication of the related samples at the correlation filter output, denoted by $\hat{y}_k$ with $k = 0, 1, \ldots, L-1$ and the preamble ω_k, to eliminate the data modulation. The operational range of the L&R estimator has a limit given by $|\nu| < 1/(K+1)$. Regarding to [9], with $K \approx L/2$, the jitter variance has a minimum.

3.2.3 Estimation of Carrier Phase and Amplitude

For carrier phase estimation, $\hat{z}_k$ is de-rotated by the frequency estimate $\hat{\nu}$. The carrier phase is computed by

$$\hat{\theta} = \arg\left(\sum_{k=0}^{L-1} \hat{z}_k e^{-j2\pi k\hat{\nu}} \right) \tag{3.27}$$

Note that the frequency error introduces an additional phase shift, which leads to a bias effect. To counteract this sort of impairment, the estimator is operated with a symmetric scheme given by

$$\hat{\theta} = \arg\left(\sum_{k=-L/2}^{L/2-1} \hat{z}_k e^{-j2\pi k\hat{\nu}} \right) \tag{3.28}$$

After having obtained the phase estimate, the amplitude estimation can be achieved by

$$\hat{A} = \mathrm{Re}\left(\frac{1}{L} \sum_{k=0}^{L-1} \hat{z}_k e^{-j(2\pi k\hat{\nu}+\hat{\theta})} \right) \tag{3.29}$$

3.3 Simulation Results

For the simulations the following parameter settings are used:

- Correlation filter bank established with nine filter elements ($m = 4$) and different resolution steps $\Delta T = 5 \times 10^{-2}, 1 \times 10^{-2}, 5 \times 10^{-3}, 1 \times 10^{-3}, 5 \times 10^{-4}, 1 \times 10^{-4}$
- Preamble: BPSK modulated pseudo-random number (PRN) sequences with different length $L = 32, 64, 128, 256, 512, 1024$ symbols
- Oversampling with $N_s = 4$
- Roll-off factor $\alpha = 0.05$ and $\alpha = 0.25$
- Normalized carrier frequency offset $\nu_s = FT_s = 0.005$ for $L \leq 256$ and $\nu_s = 0.001$ for $L > 256$ is assumed.
- AWGN and random carrier phase $\theta \in [-\pi, \pi)$

Note that for the correlation filter elements (3.18), the related waveforms are organised in a symmetric way with respect to $t = 0$. With the symmetric variant, the correlation output has a

better shape and the correlation peak lies near to the sampling grid. Thus, a lower oversampling rate (OSR) can be chosen, which is preferred due to the reasons of computational complexity.

This estimator and the other three estimation methods, which are described in the sequel, are implemented in MATLAB®.

3.3.1 Mean Estimator Value

For the mean estimator value (MEV) analysis, different symbol periods $T_m = T_0 + m\Delta T$ have been used. In the sequel, it is shown, that the performance of the correlation filter bank depends on the spacing between the filter elements and the length of the pilot sequences. Numerical results are obtained for SNR = +10 dB.

The MEV results (green dots) for three different preamble lengths and a filter element resolution $\Delta T = 5 \times 10^{-3}$, are depicted in Figures 3.2 to 3.4. It is obvious that the higher the length of the pilot sequences for a specific ΔT, the higher the performance degradation which shows a deterministic and periodic behaviour around the ideal MEV curve (blue solid line).

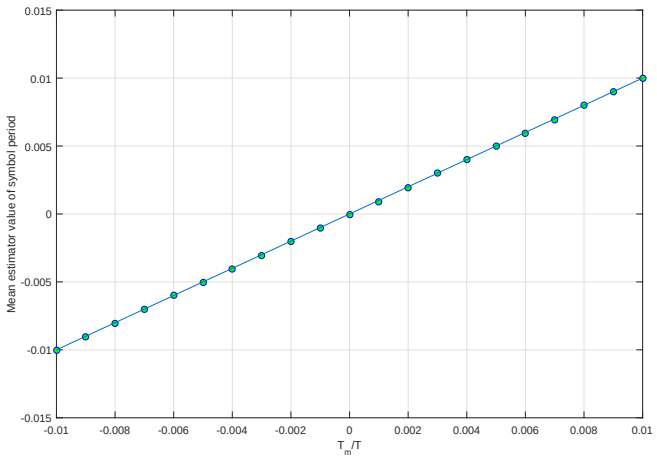

Figure 3.2: Mean estimator value ($\alpha = 0.05$, $L = 128$, $\nu_s = 0.005$, $\Delta T = 5 \times 10^{-3}$)

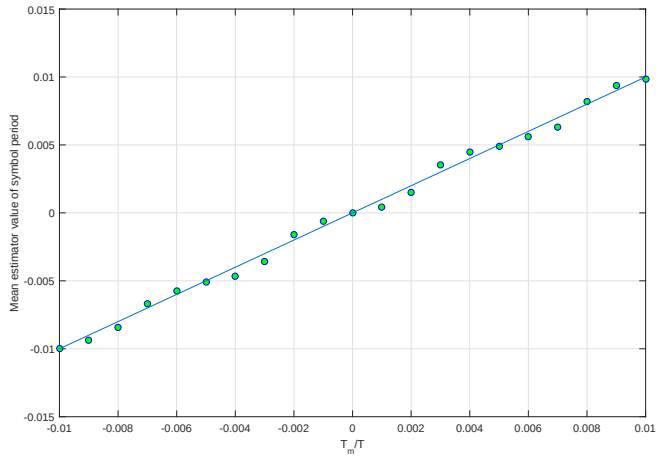

Figure 3.3: Mean estimator value ($\alpha = 0.05, L = 256, \nu_s = 0.005, \Delta T = 5 \times 10^{-3}$)

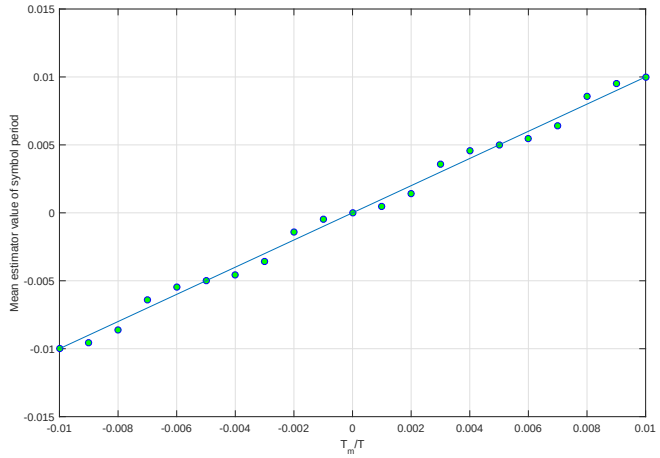

Figure 3.4: Mean estimator value ($\alpha = 0.05, L = 512, \nu_s = 0.001, \Delta T = 5 \times 10^{-3}$)

Furthermore, for $L = 128$ the MEV results for three different values of ΔT, are illustrated in Figures 3.5 to 3.7. It is clear that the lower the spacing between the correlation filter elements, the better the MEV result. As before, a deterministic and periodic performance degradation is obvious, for higher values of ΔT.

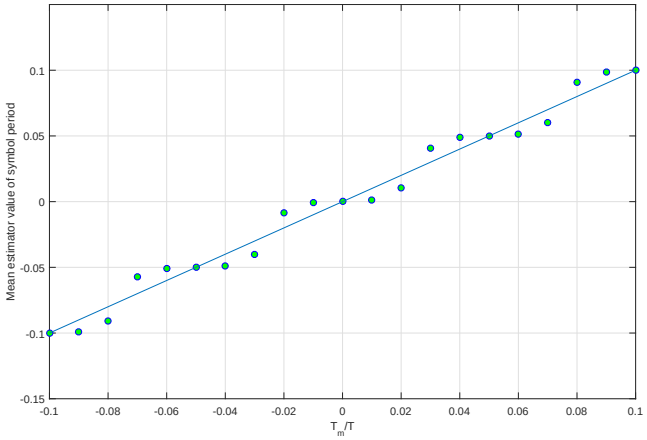

Figure 3.5: Mean estimator value ($\alpha = 0.05, L = 128, \nu_s = 0.005, \Delta T = 5 \times 10^{-2}$)

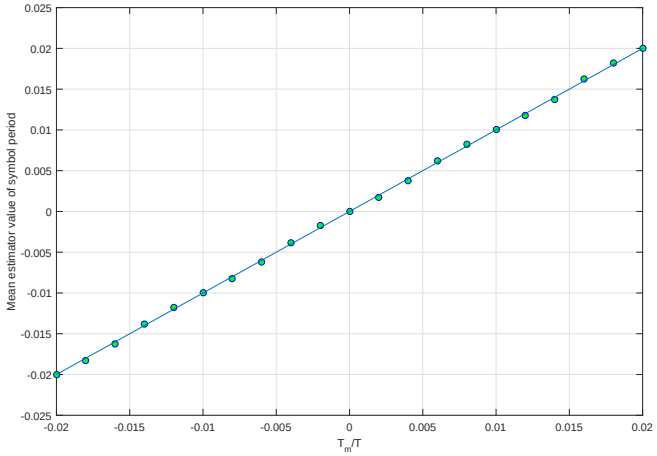

Figure 3.6: Mean estimator value ($\alpha = 0.05, L = 128, \nu_s = 0.005, \Delta T = 1 \times 10^{-2}$)

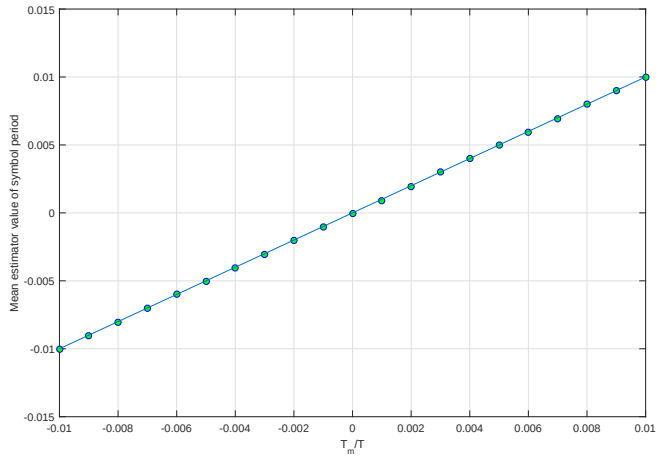

Figure 3.7: Mean estimator value ($\alpha = 0.05$, $L = 128$, $\nu_s = 0.005$, $\Delta T = 5 \times 10^{-3}$)

Summarizing, the analysis shows, that the grid ΔT has to be chosen appropriately. If it is too large, compared to the width of the main lobe, for the interpolation side lobe values are taken which leads to erroneous results. If the grid is too small, the correlation maxima values of the filter elements are too close to each other and the parabolic approach to determine the symbol rate is not longer applicable.
In addition, it was observed that for the chosen simulation settings the suitable grid spacing ΔT depends on the length of the synchronisation preamble L. For small values like $L = 64$, a spacing of $\Delta T = 1/100$ is appropriate and estimation results free from systematic errors could be achieved. For higher values like $L = 1024$, a much smaller grid $\Delta T = 1/10000$ must be applied. The total symbol rate deviation which can be covered increases linearly with the number of filter bank elements, but this leads also to an increasing complexity. These observations are true irrespective of the selected roll-off factor.

3.3.2 Jitter Variance

Due to the investigation of the MEV, it was shown that the correlation filter approach is operating well for a specific grid and preamble length. The jitter variances are computed over a SNR range from 0 dB to +30 dB. The partitioning parameter as described in (3.24) is set to $K = 4$.

Figure 3.8 and Figure 3.9 show the normalized jitter variance of the symbol timing and symbol rate using a pilot sequence with $L = 512$ symbols. It is obvious that in both cases the jitter variance is close to the MCRLB. For higher SNR values it is evident that the jitter variance

begins to flatten more and more, ending up in an error floor which can be explained due to a self noise effect caused by inter-symbol interference (ISI), regardless from AWGN. Comparing the timing and rate estimation results, the jitter floor increases with decreasing preamble length, which is depicted in Figure 3.10 and 3.11.

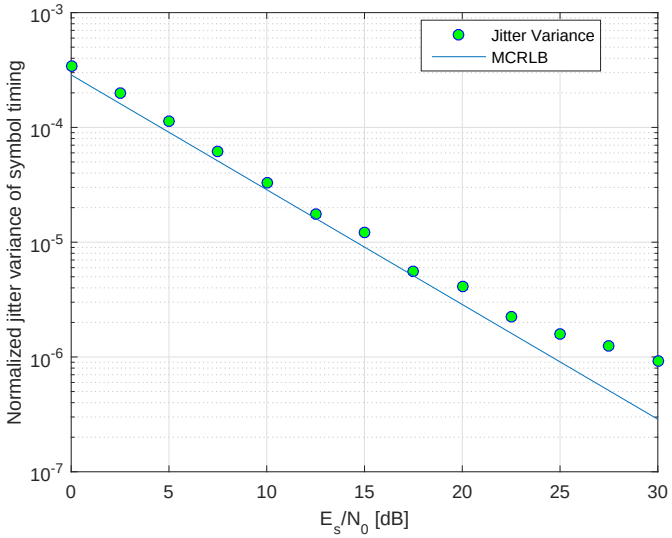

Figure 3.8: Normalized jitter variance ($\alpha = 0.25$, $L = 512$, $\nu_s = 0.001$, $\Delta T = 1 \times 10^{-3}$)

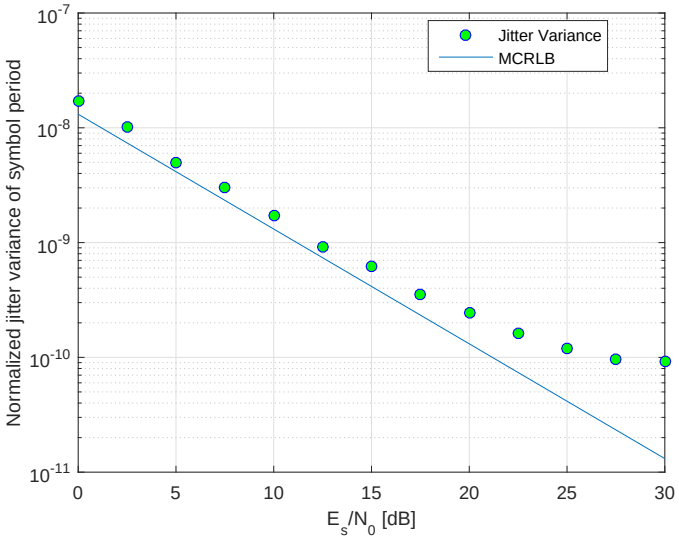

Figure 3.9: Normalized jitter variance ($\alpha = 0.25$, $L = 512$, $\nu_s = 0.001$, $\Delta T = 1 \times 10^{-3}$)

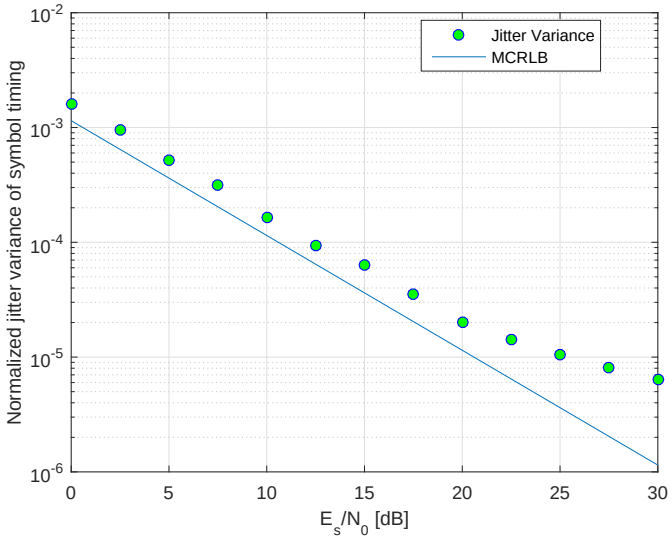

Figure 3.10: Normalized jitter variance ($\alpha = 0.25$, $L = 128$, $\nu_s = 0.005$, $\Delta T = 5 \times 10^{-3}$)

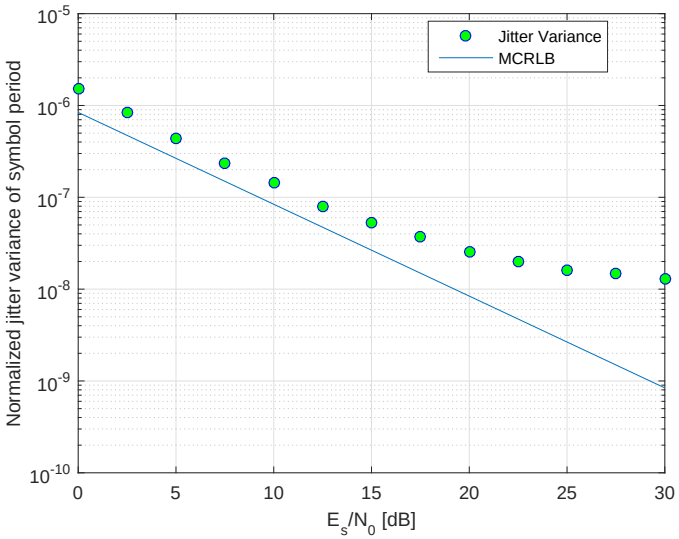

Figure 3.11: Normalized jitter variance ($\alpha = 0.25, L = 128, \nu_s = 0.005, \Delta T = 5 \times 10^{-3}$)

The simulation results also show that the performance depends on the partitioning parameter K. In Figure 3.12 and Figure 3.13 the jitter variance for the symbol timing and period for the partitioned case with $K = 4$, $L = 256$ and $\nu_s = 0.005$ is depicted. It is evident that the performance worsens which can be explained by the fact that the chosen factor K is too small to avoid the degradation by the frequency error.

The same behaviour is obvious in Figure 3.14 and Figure 3.15, which represents the jitter variances for symbol timing and period for the partitioned case with $K = 4$, $L = 1024$ and $\nu_s = 0.001$. As before the partitioning is insufficient to avoid the degradation.

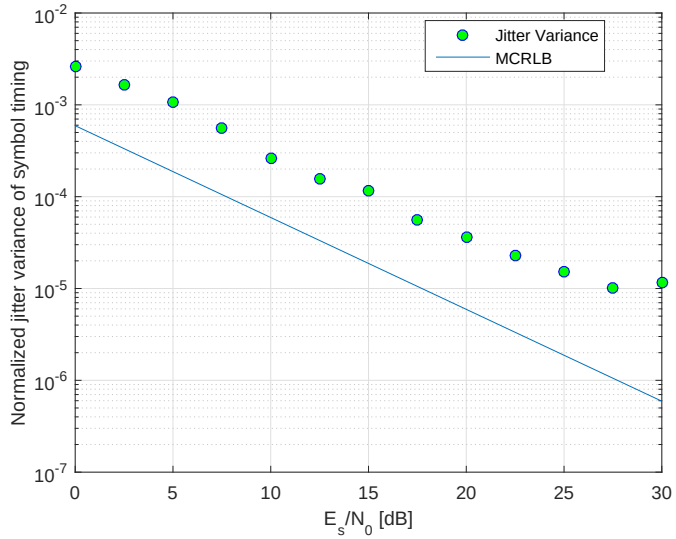

Figure 3.12: Normalized jitter variance ($\alpha = 0.05, L = 256, \nu_s = 0.005, \Delta T = 1 \times 10^{-3}$)

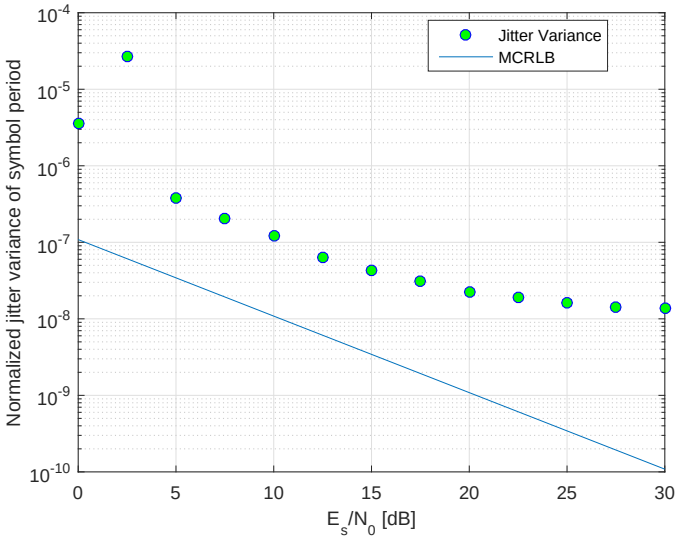

Figure 3.13: Normalized jitter variance ($\alpha = 0.05, L = 256, \nu_s = 0.005, \Delta T = 1 \times 10^{-3}$)

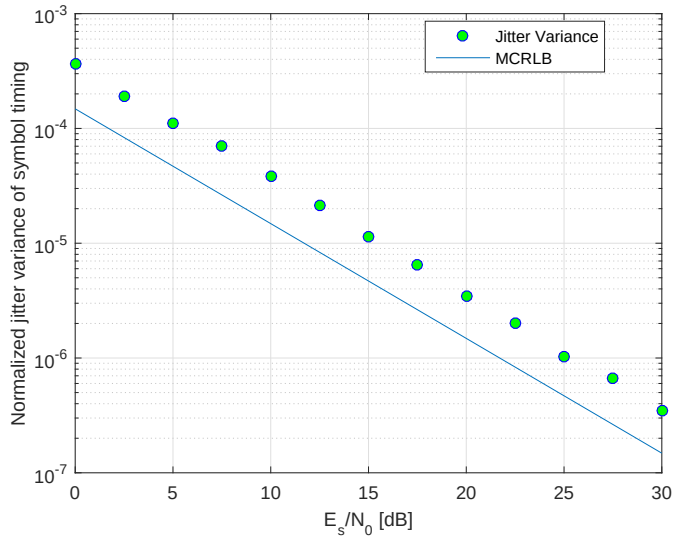

Figure 3.14: Normalized jitter variance ($\alpha = 0.05$, $L = 1024$, $\nu_s = 0.001$, $\Delta T = 1 \times 10^{-4}$)

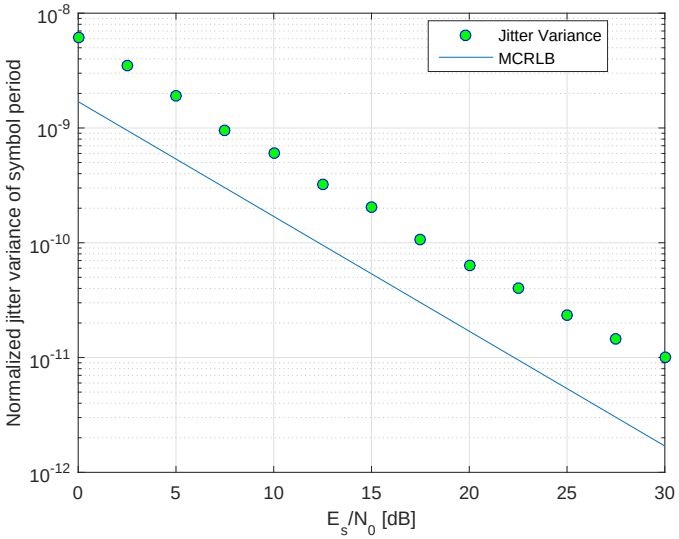

Figure 3.15: Normalized jitter variance ($\alpha = 0.05$, $L = 1024$, $\nu_s = 0.001$, $\Delta T = 1 \times 10^{-4}$)

To demonstrate that the performance degradation is caused by insufficient partitioning, the frequency error for both lengths is reduced. Therefore, for $L = 256$ a frequency error of $\nu_s = 0.0025$ and for $L = 1024$ a frequency error of $\nu_s = 0.0005$ is assumed. For both cases, $K = 4$ parts are chosen. Figure 3.16 to Figure 3.19 demonstrates the expected results that for

lower frequency errors better results can be achieved. The symbol timing and rate estimates are closer to the MCRLB than before.

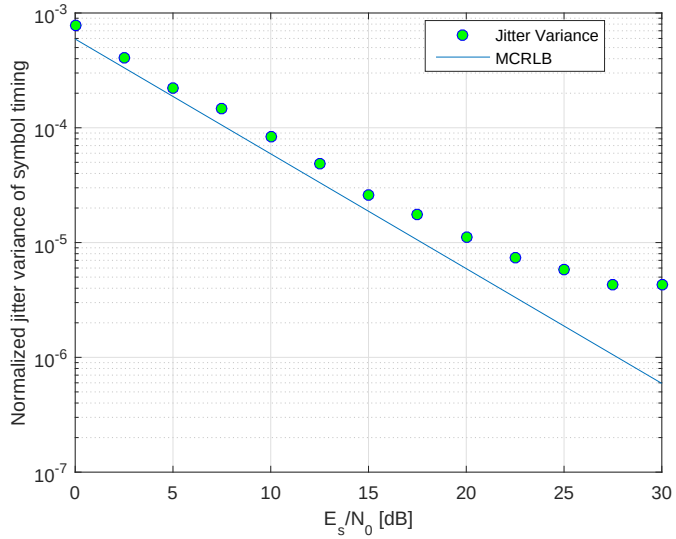

Figure 3.16: Normalized jitter variance ($\alpha = 0.05$, $L = 256$, $\nu_s = 0.0025$, $\Delta T = 1 \times 10^{-3}$)

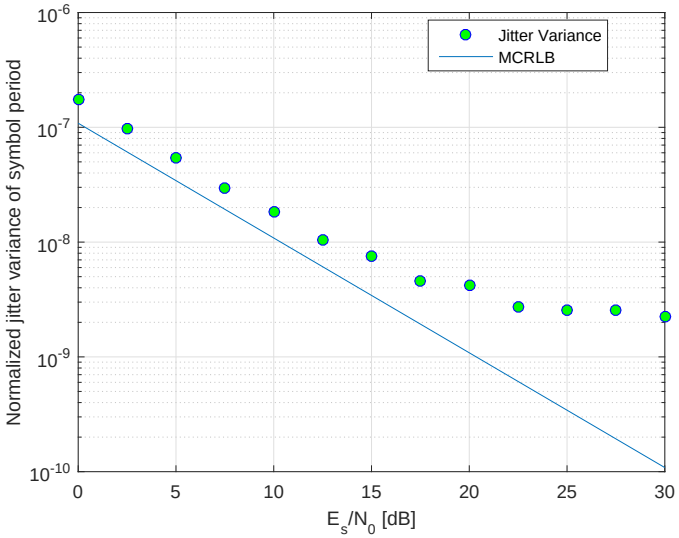

Figure 3.17: Normalized jitter variance ($\alpha = 0.05$, $L = 256$, $\nu_s = 0.0025$, $\Delta T = 1 \times 10^{-3}$)

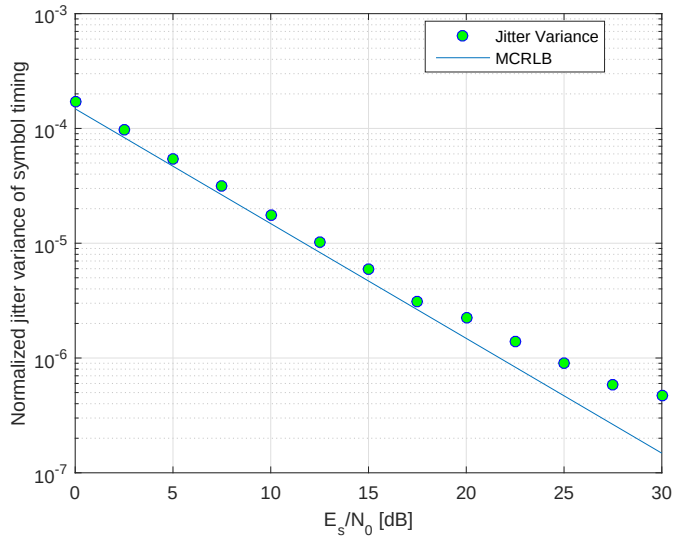

Figure 3.18: Normalized jitter variance ($\alpha = 0.05, L = 1024, \nu_s = 0.0005, \Delta T = 1 \times 10^{-4}$)

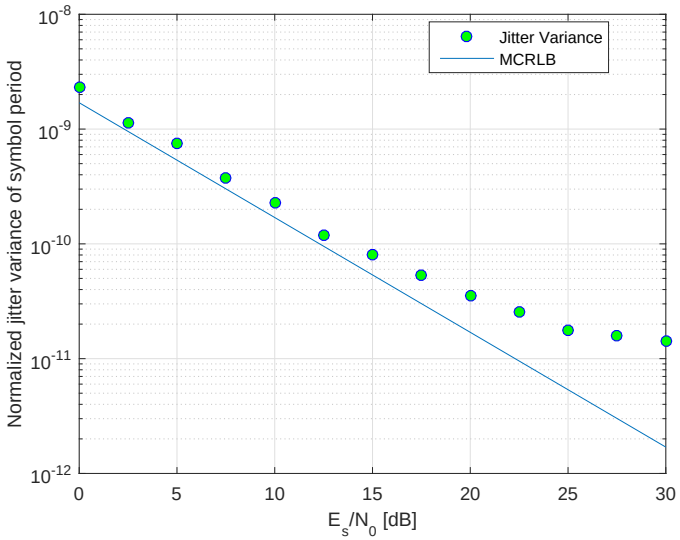

Figure 3.19: Normalized jitter variance ($\alpha = 0.05, L = 1024, \nu_s = 0.0005, \Delta T = 1 \times 10^{-4}$)

Furthermore, the investigation of all simulation cases shows that, regardless of the pilot sequence length L or roll-off factor α, the jitter variances of ν_s, θ and A are close to the MCRLB. Hence, the estimation after symbol timing and rate recovery is working properly. This is shown in Figures 3.20 to 3.22.

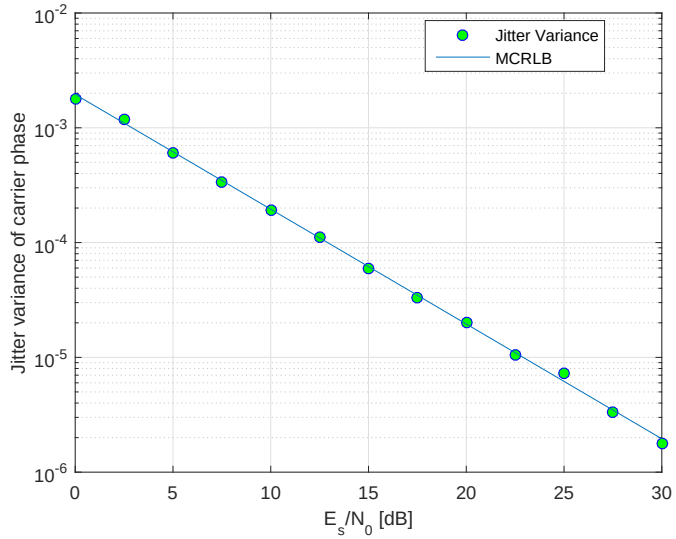

Figure 3.20: Jitter variance ($\alpha = 0.25, L = 256, \nu_s = 0.005, \Delta T = 5 \times 10^{-4}$)

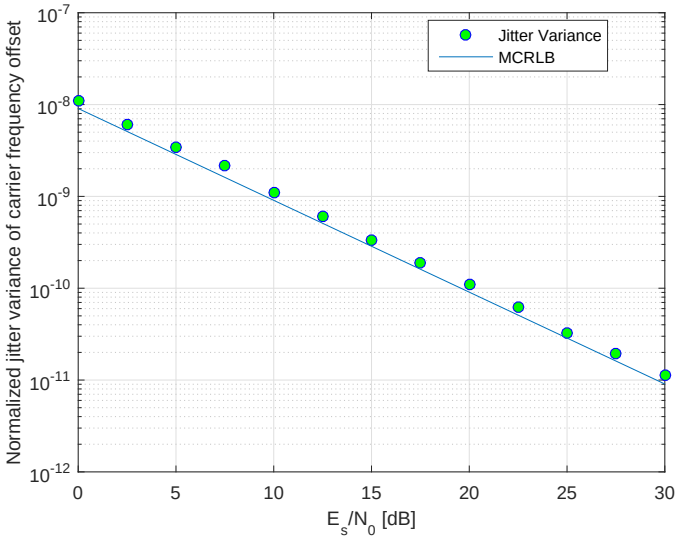

Figure 3.21: Normalized jitter variance ($\alpha = 0.25, L = 256, \nu_s = 0.005, \Delta T = 5 \times 10^{-4}$)

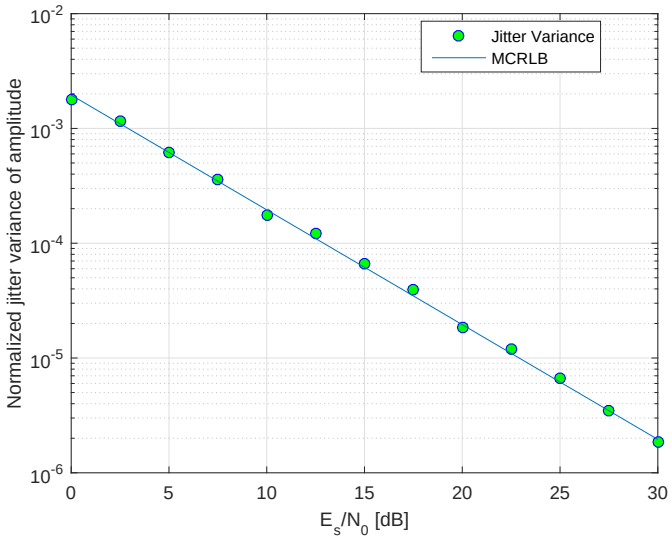

Figure 3.22: Normalized jitter variance ($\alpha = 0.25, L = 256, \nu_s = 0.005, \Delta T = 5 \times 10^{-4}$)

4 Symbol Rate Estimation by Timing Estimation - Data-Aided Variant

4.1 Estimator Approach and Algorithm

This symbol rate estimation method is based on the following principle: The symbol timing of two pilot sequences with length $L/2$, separated by a payload data packet with length N, is estimated. With these estimates, the drift per symbol will be computed. The data structure model is shown in Figure 4.1.

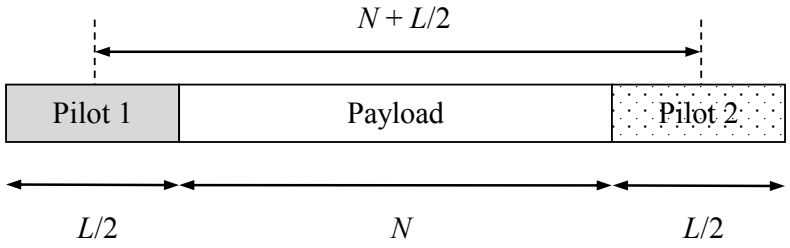

Figure 4.1: Data structure for parameter estimation

Note, that a very small drift size is assumed, hence the symbol timing estimation is not affected.

As described in Chapter 3, the symbol timings of the two pilot sequences are estimated via a parabolic interpolation of the correlation main lobe, given by

$$\hat{\tau}_1 = \left(\hat{\mu}_1 - \frac{1}{2} \frac{Y_{\hat{\mu}_1+1} - Y_{\hat{\mu}_1-1}}{Y_{\hat{\mu}_1+1} - 2Y_{\hat{\mu}_1} + Y_{\hat{\mu}_1-1}} \right) T_s \tag{4.1}$$

$$\hat{\tau}_2 = \left(\hat{\mu}_2 - \frac{1}{2} \frac{Y_{\hat{\mu}_2+1} - Y_{\hat{\mu}_2-1}}{Y_{\hat{\mu}_2+1} - 2Y_{\hat{\mu}_2} + Y_{\hat{\mu}_2-1}} \right) T_s \tag{4.2}$$

The drift per symbol is computed as follows:

$$\Delta T = \frac{[[\hat{\tau}_2]_{\pm T/2} - [\hat{\tau}_1]_{\pm T/2}]_{\pm T/2}}{N + L/2} \tag{4.3}$$

4.2 Modified Cramer-Rao Lower Bound and Jitter Variance

Symbol Timing

The jitter variance of the symbol timing of each pilot sequence is approximated by the modified Cramer-Rao lower bound (derived in Chapter 3) of the symbol timing of each preamble and is denoted as

$$\sigma_\tau^2 \approx \mathrm{MCRLB}(\tau) = -\frac{1}{L\gamma_s T^2 \ddot{g}(0)} \tag{4.4}$$

Symbol Period

The jitter variance of the symbol period results from the residual symbol timing error and can be expressed by

$$\sigma_\eta^2 = \frac{2\sigma_\tau^2}{(N + L/2)^2} = -\frac{1}{L/2(N + L/2)^2 \gamma_s T^2 \ddot{g}(0)} \tag{4.5}$$

The mathematical derivation of the MCRLB leads to the following formula:

$$\mathrm{MCRLB}(\eta) = -\frac{3}{L/2[4(L/2)^2 + 3N^2 + 3LN - 1]\gamma_s T^2 \ddot{g}(0)} \tag{4.6}$$

4.3 Simulation Results

For the simulations the following parameter settings are used:

- Pilot sequences: BPSK modulated PRN sequences with different length $L/2 = 16, 32, 64, 128$
- Payload: BPSK modulated PRN sequence with $N = 1024$ symbols
- Oversampling with $N_s = 4$
- Roll-off factor $\alpha = 0.05$ and $\alpha = 0.25$
- Normalized residual frequency error $\sqrt{\mathrm{MCRLB}(\nu)}$

- AWGN and random carrier phase $\theta \in [-\pi, \pi)$

It is assumed that the carrier frequency offset was already estimated, corrected and only a residual frequency error exists.

4.3.1 Normalized Jitter Variance

For this estimator approach only the normalized jitter variance of the symbol timing and symbol period is computed. Figures 4.2, 4.4 and 4.6 show the normalized jitter variance for timing and Figures 4.3, 4.5 and 4.7 for period. It is obvious that a short pilot length delivers a degraded performance in the lower SNR range. This can be explained due to the fact that the used algorithm is not linear, so the smaller the preamble length, the higher the noise components. It is also obvious that the variance ends up earlier in a jitter floor. This error floor is caused by a self-noise effect, regardless from the AWGN component. In Figures 4.4 to 4.7 the variances for higher preamble length are illustrated and it is apparent that the jitter variances are close to the MCRLB in lower SNR range and then end up into an error floor. Furthermore, it is evident that increasing pilot sequence length leads to a decreased the jitter floor.

For a much smaller roll-off factor given by $\alpha = 0.05$, no significant differences could be observed.

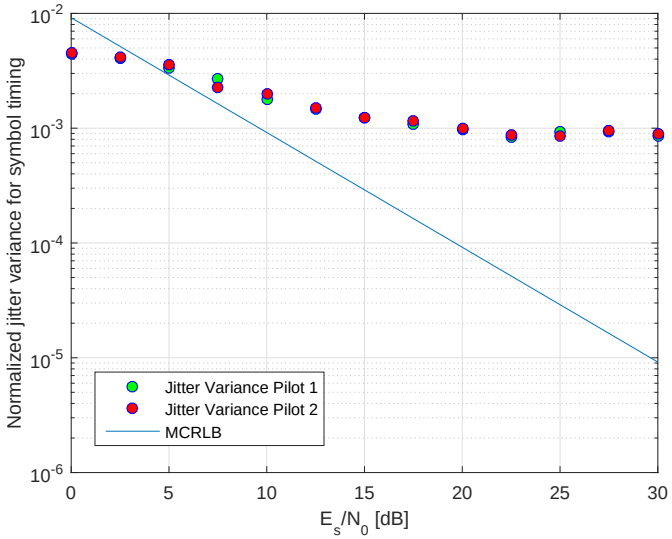

Figure 4.2: Normalized jitter variance ($\alpha = 0.25, L/2 = 16$)

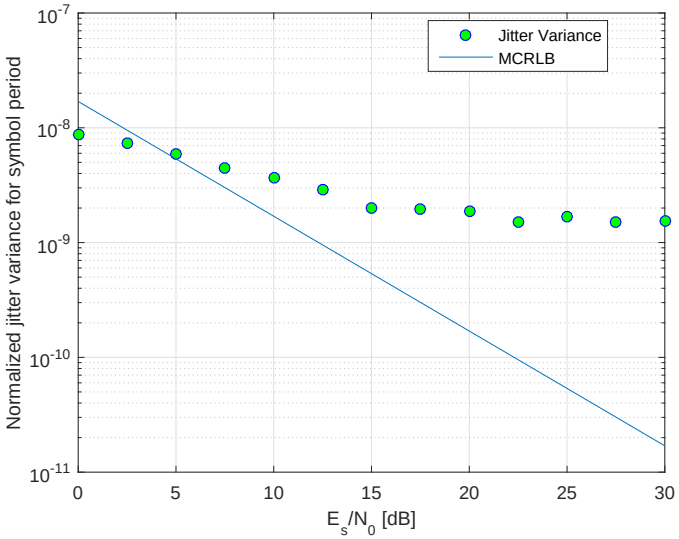

Figure 4.3: Normalized jitter variance ($\alpha = 0.25, L/2 = 16$)

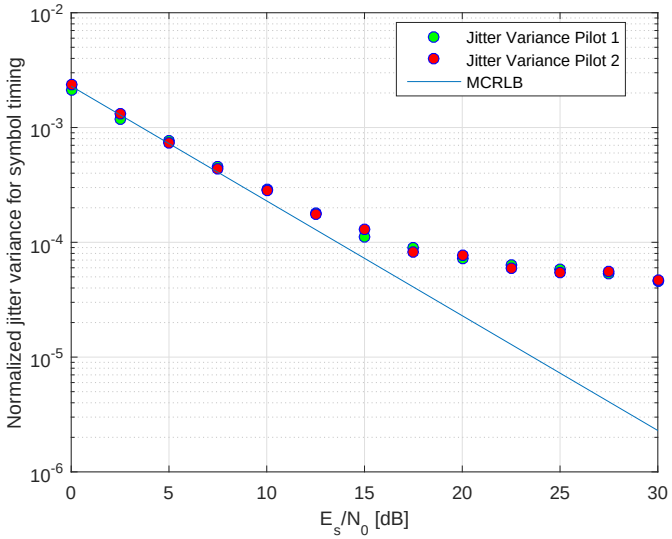

Figure 4.4: Normalized jitter variance ($\alpha = 0.25, L/2 = 64$)

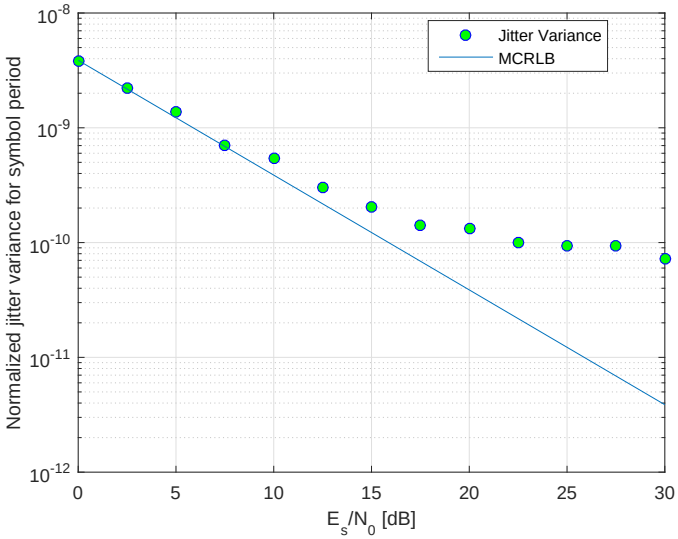

Figure 4.5: Normalized jitter variance ($\alpha = 0.25, L/2 = 64$)

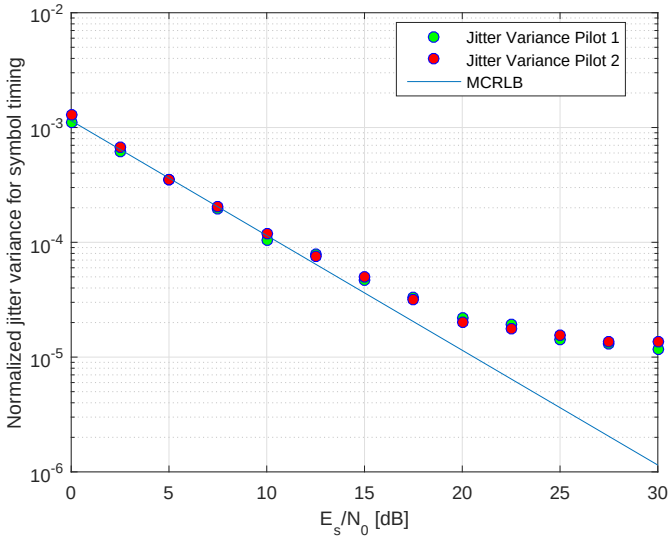

Figure 4.6: Normalized jitter variance ($\alpha = 0.25, L/2 = 128$)

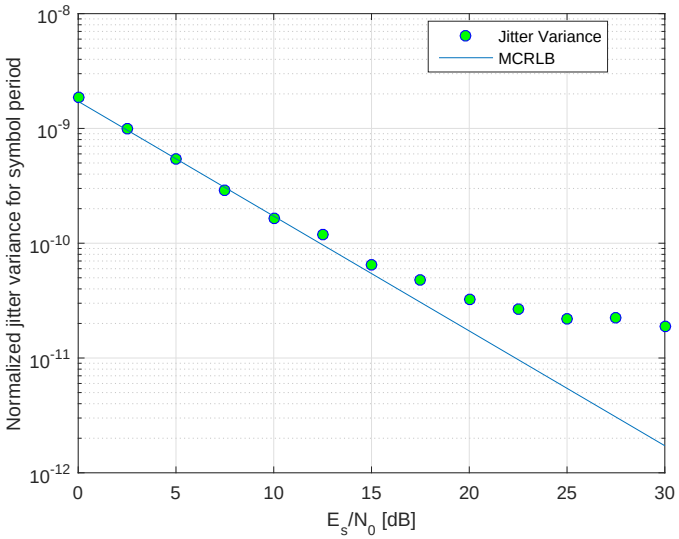

Figure 4.7: Normalized jitter variance ($\alpha = 0.25, L/2 = 128$)

5 Symbol Rate Estimation by Timing Estimation - Combined Data-Aided/Non- Data-Aided Variant

5.1 Estimator Approach

For this method a feedforward scheme, using a hybrid data-aided (DA)/non-data-aided (NDA) method is assumed. Regarding to [10], for the symbol timing recovery and symbol rate estimation respectively a dual-filter framework is used. This framework includes a matched filter (MF), a derivative matched filter (DMF), and a NDA estimator. Note that the estimator assumes only residual errors. The dual-filter model is shown in Figure 5.1.

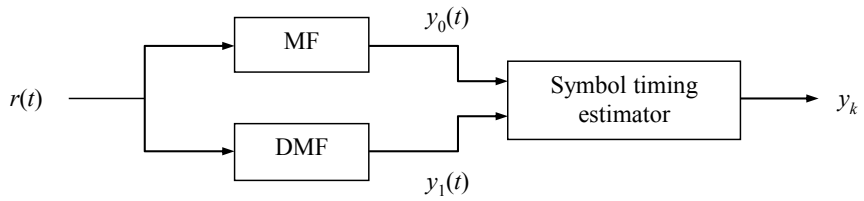

Figure 5.1: FF scheme for NDA estimation

It is assumed that the carrier frequency offset is already estimated, corrected and only a residual frequency error exists, denoted by $\Delta F = |F - \hat{F}| << 1$. Therefore, the corrected signal can be expressed by

$$r'(t) = e^{-j2\pi\hat{F}t}\, r(t) \tag{5.1}$$

It is obvious that $r'(t)$ passes the MF and the DMF. So the corresponding output signal samples at both filters can be written as follows:

$$y_{0,k} = r'(t) \otimes h(t)|_{t=kT} \tag{5.2}$$

$$y_{1,k} = r'(t) \otimes h_1(t)|_{t=kT} \tag{5.3}$$

where $h(t)$ is the impulse response of the MF and $h_1(t)$ is the impulse response of the DMF.

As described in [10], the NDA estimator computes the symbol timing as follows:

$$\hat{\tau} = \frac{T}{2\pi}\arg(U_0 + jU_1) \tag{5.4}$$

where U_0 is given by

$$U_0 = \cos(2\pi\epsilon) \approx \frac{4}{\alpha L}\sum_{k=0}^{L/2-1}\left(|y_{0,k}|^2 - |y_{0,k-1/2}|^2\right) \tag{5.5}$$

and U_1 is given by

$$U_1 = \sin(2\pi\epsilon) \approx \frac{6\pi}{L}\sum_{k=0}^{L/2-1}\mathrm{Re}[y_{0,k}^* y_{1,k}] \tag{5.6}$$

where $y_{0,k}$ and $y_{1,k}$ are the samples in the middle of the symbol. Therefore, the estimation result depends of the chosen samples.

5.2 Modified Cramer-Rao Lower Bound and Jitter Variance

Symbol Timing

The jitter variance of the symbol timing of the DA estimator is approximated by the modified Cramer-Rao lower bound (derived in Chapter 3) of the symbol timing and can be denoted as,

$$\sigma_{\tau,1}^2 \approx \mathrm{MCRLB}(\tau) = -\frac{1}{L\gamma_s T^2 \ddot{g}(0)} \tag{5.7}$$

and the jitter variance of the timing for a ML-NDA algorithm is derived as follows [10]:

$$\sigma_{\tau,2}^2 \approx \sigma_{\text{ML-NDA}}^2 = \frac{1}{\alpha\pi^2\gamma_s L/2} \tag{5.8}$$

Symbol Period

The jitter variance of the symbol period results from the jitter variances of the DA and NDA estimator and can be expressed by

$$\sigma_\eta^2 = \frac{\sigma_{\tau,1}^2 + \sigma_{\tau,2}^2}{(N + L/2)^2} \tag{5.9}$$

The MCRLB for the symbol period is the same as derived in Chapter 4:

$$\mathrm{MCRLB}(\eta) = -\frac{3}{L/2[4(L/2)^2 + 3N^2 + 3LN - 1]\gamma_s T^2 \ddot{g}(0)} \tag{5.10}$$

5.3 Oerder-Meyr Algorithm

The performance of the investigated estimator is compared with the standard Oerder-Meyr (O&M) algorithm [11]. This algorithm estimates the symbol timing as follows: In the first step a simple discrete Fourier transformation (DFT) is carried out which is expressed by

$$X_L = \sum_{k=0}^{N_s L/2-1} |y_k|^2 e^{-j2\pi k/N_s} \tag{5.11}$$

where y_k are the output samples at the MF. In the second step the symbol timing is estimated by

$$\hat{\tau} = \frac{T}{2\pi}\arg(X_L) \tag{5.12}$$

Note that for O&M algorithms an oversampling rate $N_s = 4$ is normally suggested.

5.4 Simulation Results

For the simulations the following parameter settings are used:

- Pilot sequences: QPSK or 16-APSK modulated PRN sequences with different length $L/2 = 50, 125, 250, 500$
- Oversampling with $N_s = 4$
- Roll-off factor $\alpha = 0.05$ and $\alpha = 0.25$
- Normalized residual frequency error $\sqrt{\mathrm{MCRLB}(\nu)}$
- AWGN and random carrier phase $\theta \in [-\pi, \pi)$

5.4.1 Normalized Jitter Variance

For this estimator approach, only the normalized jitter variance of the timing and period is determined. Comparing the charts for symbol timing and symbol period variance, it is clear that the symbol timing estimation results are a function of the length value $L/2$ and α. Comparing the

Figures 5.2 to 5.5 with the Figures 5.6 to 5.9 shows that the lower α, the higher is the degradation of the performance. This can be explained by the fact that the NDA estimator is sensitive to the roll-off factor. This sensitivity also explains the distance between MCRLB and ML-NDA bound and the fact that it decreases with higher α values. With a very low roll-off factor, given by $\alpha = 0.05$, it is obvious in Figures 5.2 to 5.5 that with higher preamble lengths, the jitter variance is getting closer to the ML-NDA bound and the jitter floor decreases. Illustrated in Figures 5.6 to 5.9, for a much higher roll-off factor, given by $\alpha = 0.25$, the jitter variance of the timing estimates does not end up in a noise floor at higher SNR values, regardless the length. Also, it is visible that in the lower SNR range the variance is not close to the ML-NDA bound.

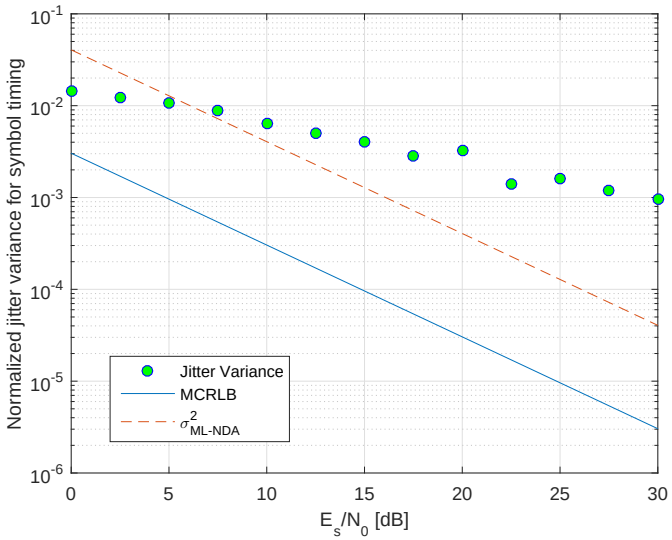

Figure 5.2: Normalized jitter variance for 16-APSK ($\alpha = 0.05, L/2 = 50$)

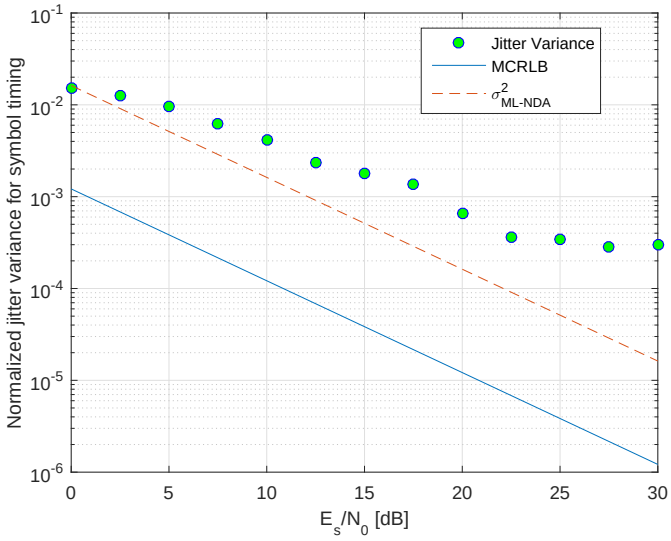

Figure 5.3: Normalized jitter variance for 16-APSK ($\alpha = 0.05, L/2 = 125$)

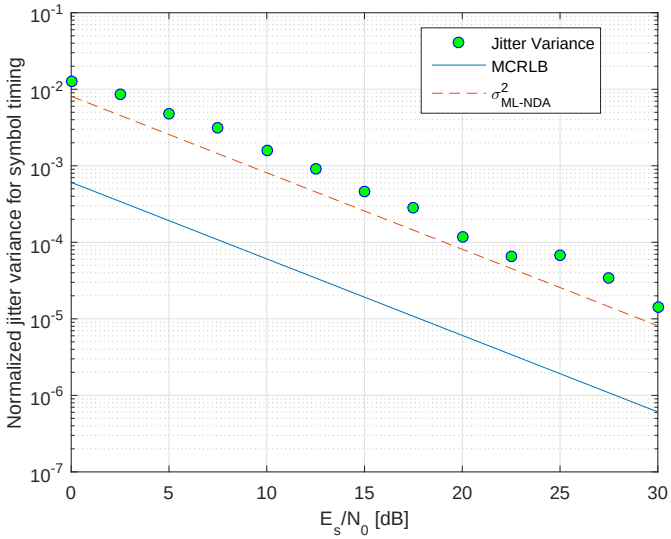

Figure 5.4: Normalized jitter variance for 16-APSK ($\alpha = 0.05, L/2 = 250$)

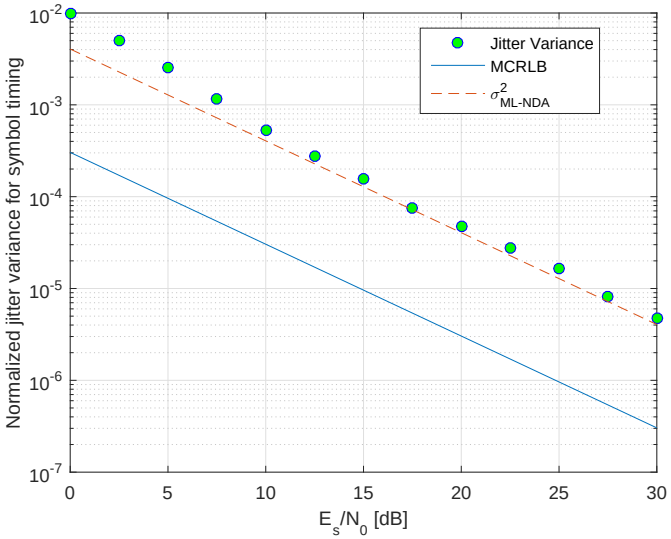

Figure 5.5: Normalized jitter variance ($\alpha = 0.05, L/2 = 500$)

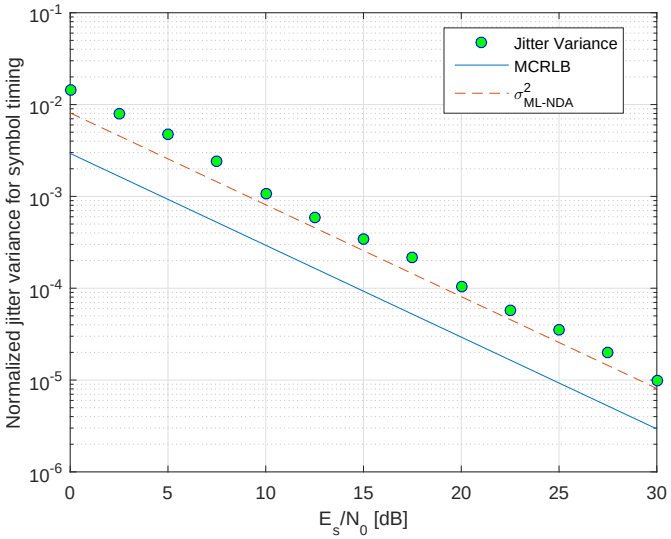

Figure 5.6: Normalized jitter variance for 16-APSK ($\alpha = 0.25, L/2 = 50$)

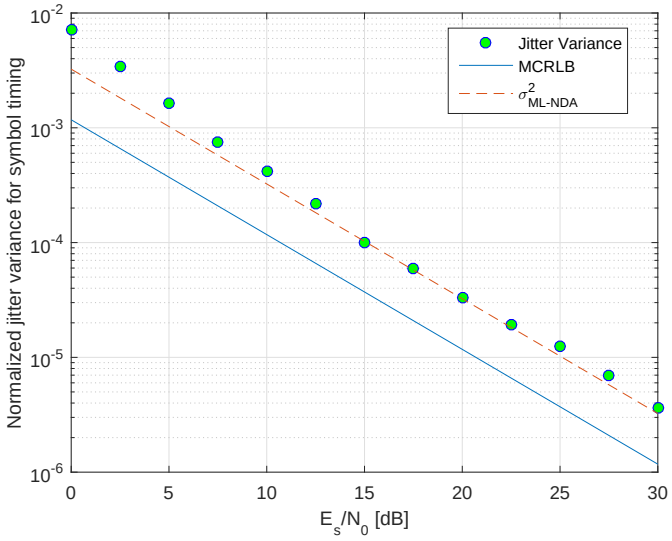

Figure 5.7: Normalized jitter variance for 16-APSK ($\alpha = 0.25, L/2 = 125$)

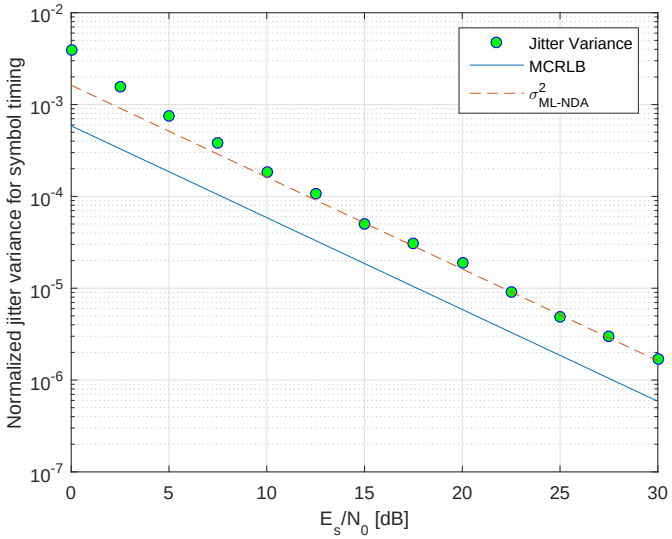

Figure 5.8: Normalized jitter variance for 16-APSK ($\alpha = 0.25, L/2 = 250$)

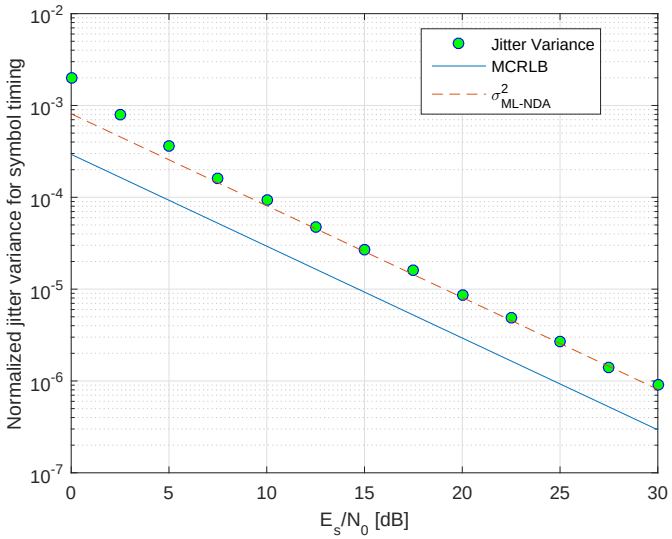

Figure 5.9: Normalized jitter variance for 16-APSK ($\alpha = 0.25, L/2 = 500$)

In Figures 5.10 to 5.13 results of the symbol rate variance are depicted. They show that the variance of the timing estimates has an offset to the MCRLB which depends on the roll-off factor. This can be explained by the fact that the lower α, the worse the performance of the NDA estimator. The results for a small roll-off factor, given by $\alpha = 0.05$, are illustrated in Figures 5.10 and 5.11. Again there is no length dependency. Figures 5.12 and 5.13 demonstrate that higher roll-off factors lead to results closer to the MCRLB.

For QPSK modulated data, no significant differences could be observed.

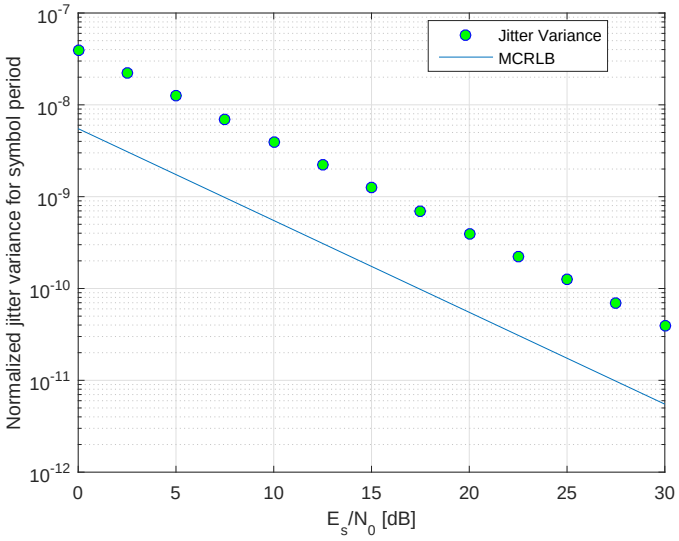

Figure 5.10: Normalized jitter variance for 16-APSK ($\alpha = 0.05, L/2 = 50$)

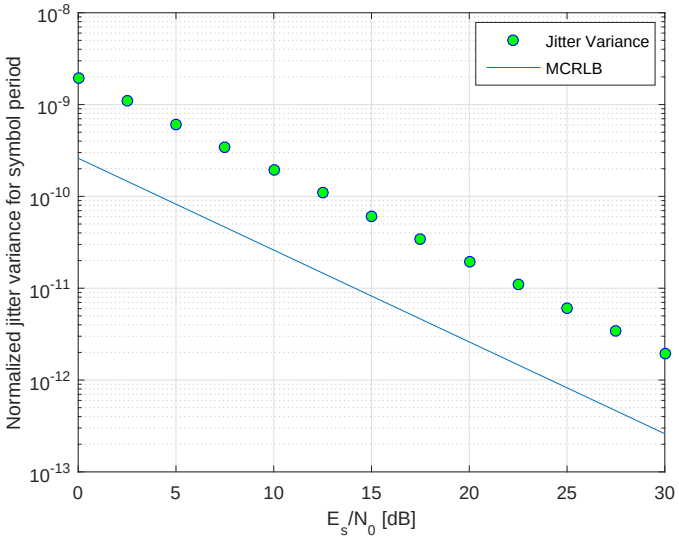

Figure 5.11: Normalized jitter variance for 16-APSK ($\alpha = 0.05, L/2 = 500$)

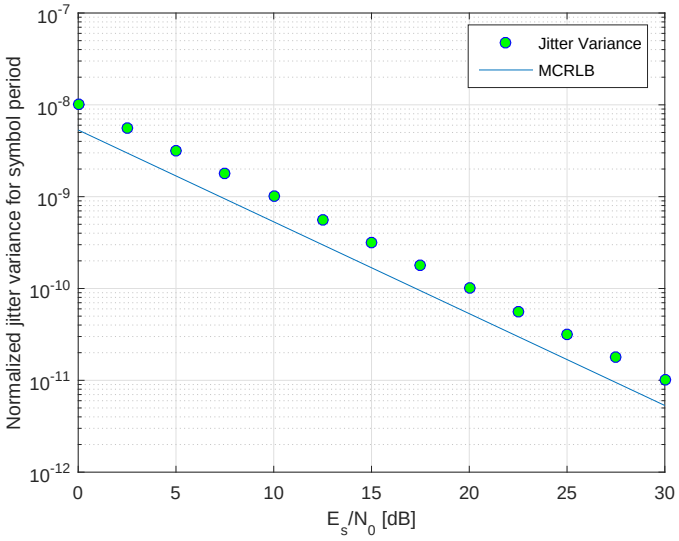

Figure 5.12: Normalized jitter variance for 16-APSK ($\alpha = 0.25, L/2 = 50$)

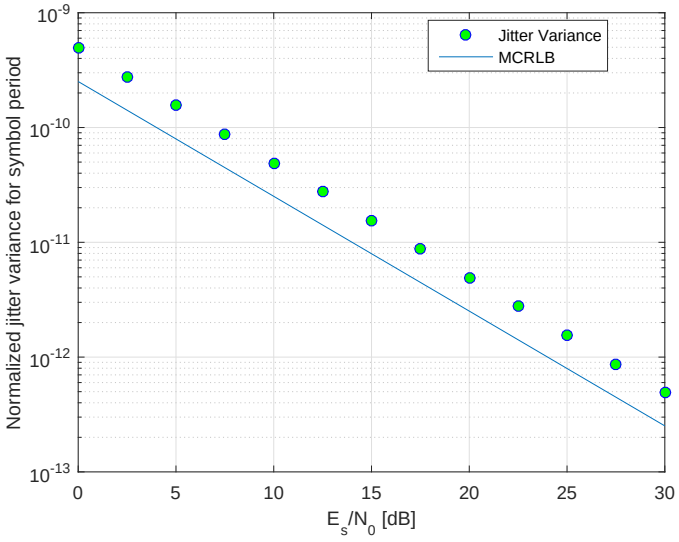

Figure 5.13: Normalized jitter variance for 16-APSK ($\alpha = 0.25, L/2 = 500$)

In the sequel, the results of the combined DA/NDA approach implemented as FF scheme are compared with the standard Oerder-Meyr algorithm. Note that for O&M an oversampling of $N_s = 4$ is assumed. Comparing to the simulation results of the timing variances, Figures 5.14 to 5.17 and Figures 5.18 to 5.21 reveal that all O&M results end up in an error floor, due to a self-noise effect which was already described in the previous chapter. Also, it is clear that the jitter floor decreases with increasing α and length value. For comparison reason, the ML-NDA bound is also shown in the charts.

Figures 5.22 to 5.25 show some results of the symbol period variance. It is obvious, the O&M algorithm delivers similar results, as well as the DA/NDA approach. Again, for QPSK modulated data, no significant differences could be observed.

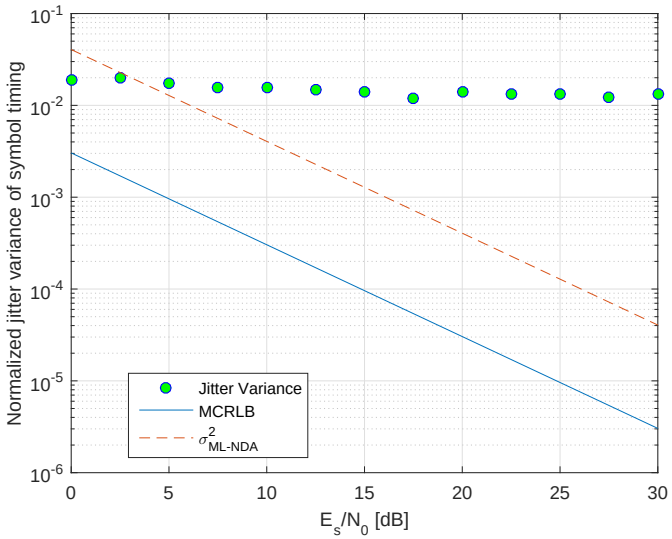

Figure 5.14: Normalized jitter variance for 16-APSK ($\alpha = 0.05, L/2 = 50$)

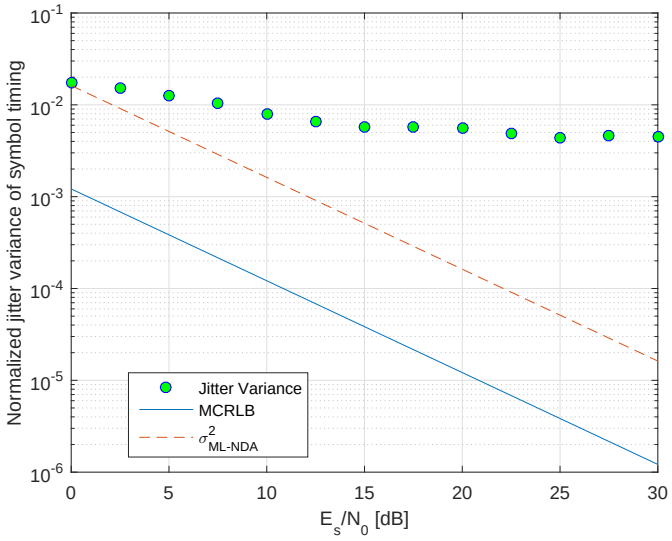

Figure 5.15: Normalized jitter variance for 16-APSK ($\alpha = 0.05, L/2 = 125$)

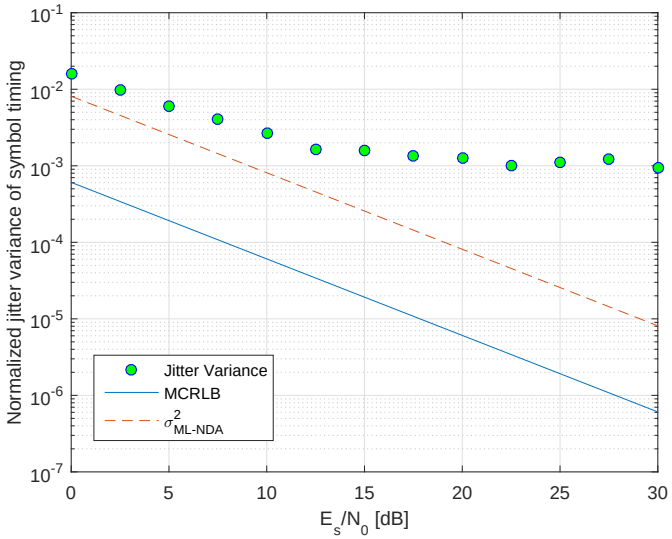

Figure 5.16: Normalized jitter variance for 16-APSK ($\alpha = 0.05, L/2 = 250$)

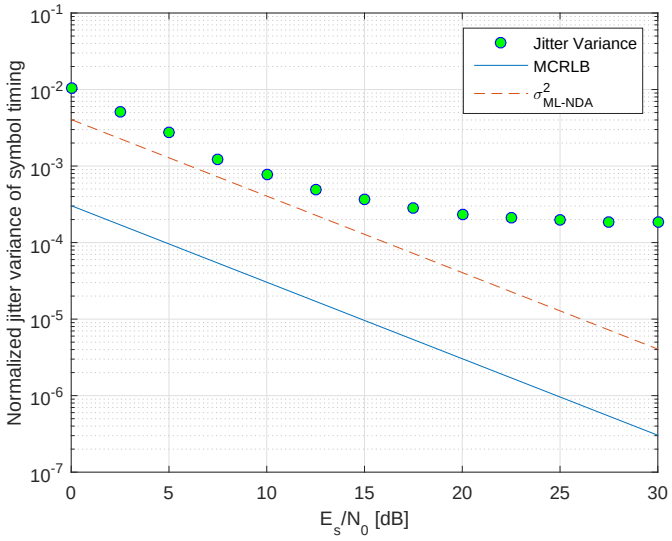

Figure 5.17: Normalized jitter variance for 16-APSK ($\alpha = 0.05, L/2 = 500$)

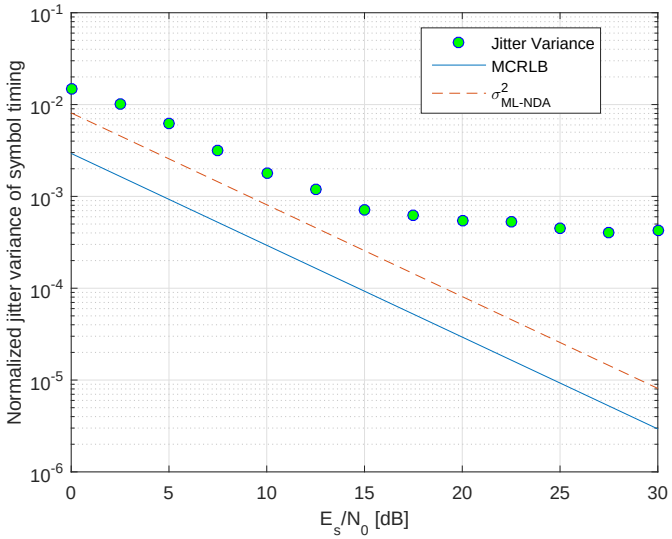

Figure 5.18: Normalized jitter variance for 16-APSK ($\alpha = 0.25, L/2 = 50$)

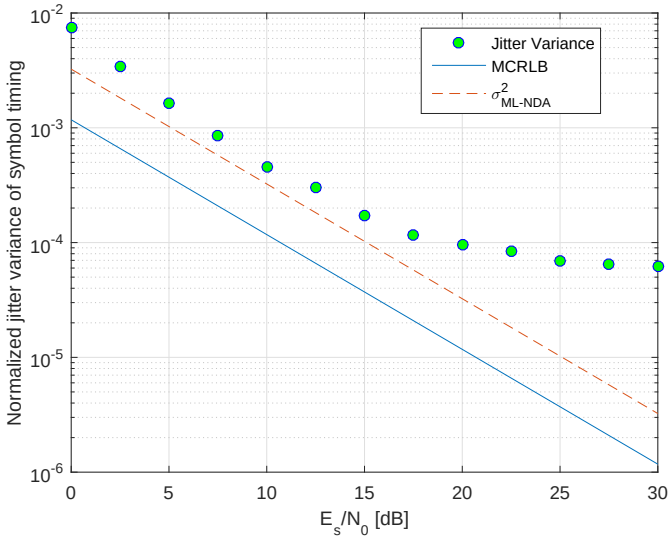

Figure 5.19: Normalized jitter variance for 16-APSK ($\alpha = 0.25, L/2 = 125$)

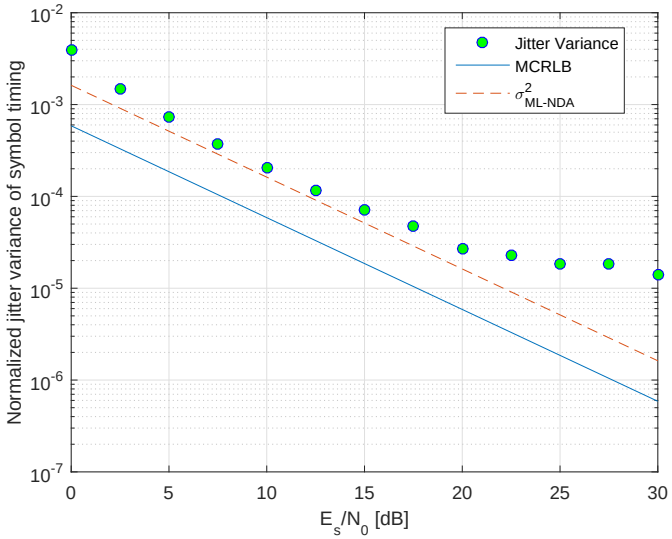

Figure 5.20: Normalized jitter variance for 16-APSK ($\alpha = 0.25, L/2 = 250$)

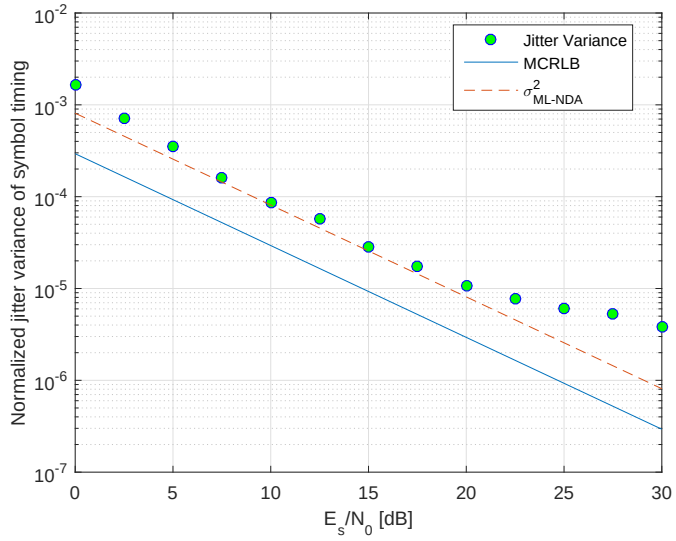

Figure 5.21: Normalized jitter variance for 16-APSK ($\alpha = 0.25, L/2 = 500$)

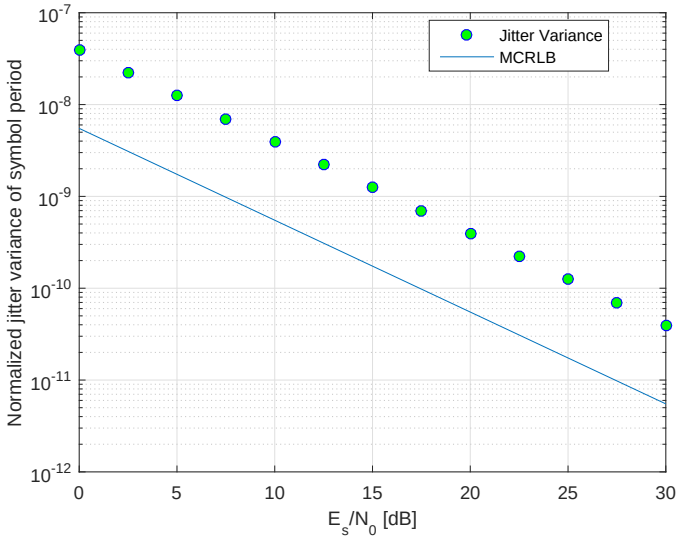

Figure 5.22: Normalized jitter variance for 16-APSK ($\alpha = 0.05, L/2 = 50$)

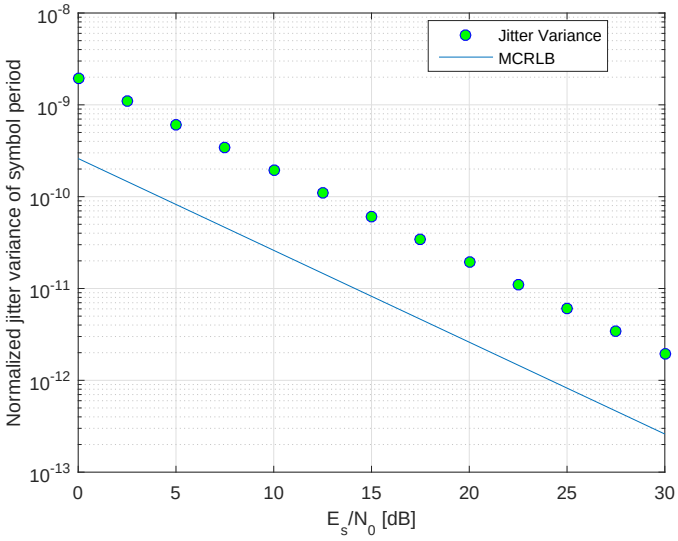

Figure 5.23: Normalized jitter variance for 16-APSK ($\alpha = 0.05, L/2 = 500$)

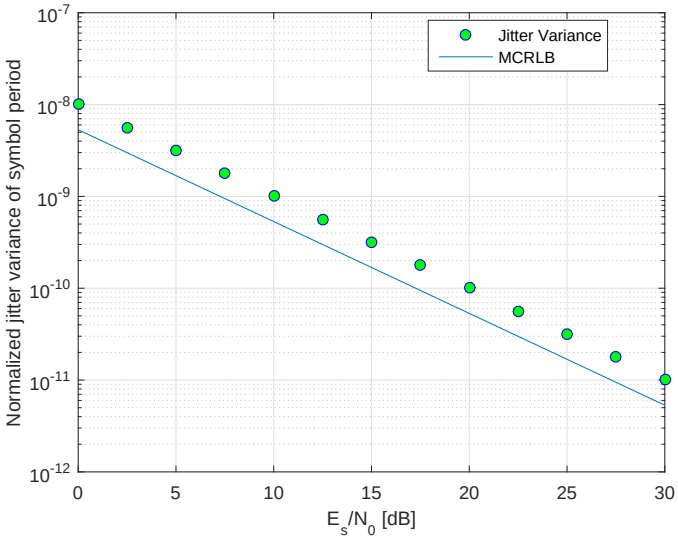

Figure 5.24: Normalized jitter variance for 16-APSK ($\alpha = 0.25, L/2 = 50$)

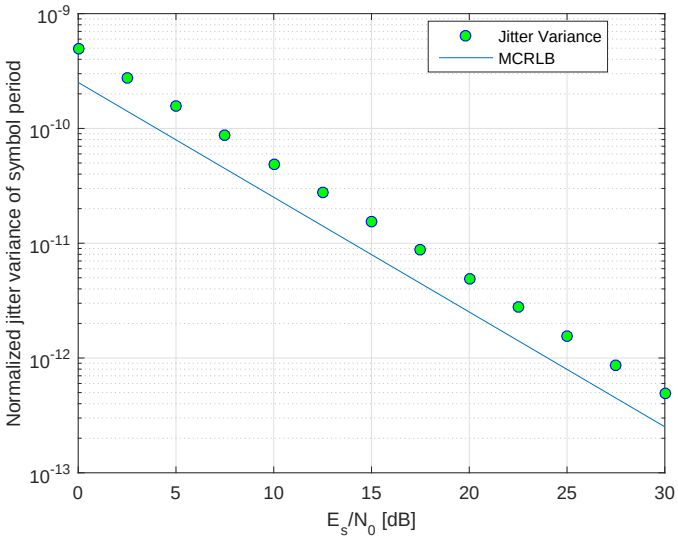

Figure 5.25: Normalized jitter variance for 16-APSK ($\alpha = 0.25, L/2 = 500$)

The comparison of both estimators show that the investigated estimator approach delivers a better performance for symbol timing estimation than the one using the O&M algorithm. Both deliver similar results for the symbol period estimation.

6 Carrier-Blind Non-Data-Aided Tracking

6.1 Estimator Approach

A feedback solution, in this work implemented as phased-locked loop (PLL), is an attractive method to track small deviations from the stable equilibrium point. As already described in [10], the recovery scheme is implemented in form of a FB scheme using the dual-filter framework introduced in Chapter 5. Figure 6.1 shows the block diagram of the synchroniser.

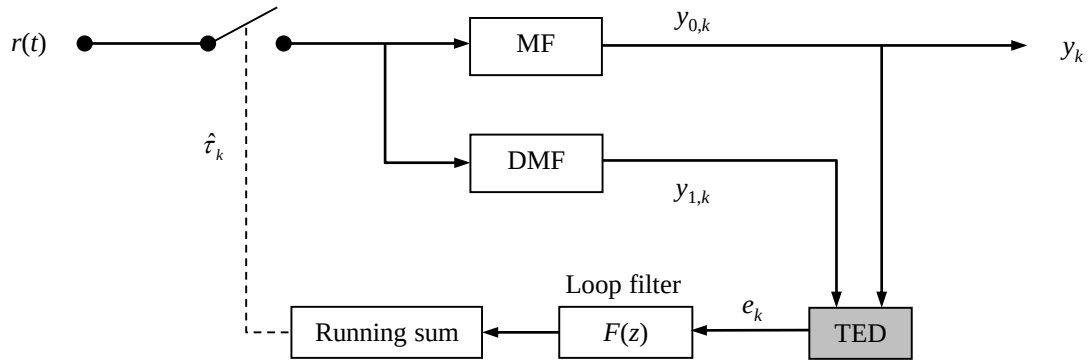

Figure 6.1: FB scheme for symbol timing recovery

Like in Chapter 5, it is assumed that the carrier frequency offset is already estimated, corrected and only a residual frequency error exists, denoted by $\Delta F = |F - \hat{F}| << 1$. Therefore, the corrected signal can be expressed by

$$r'(t) = e^{-j2\pi\hat{F}t}\, r(t) \tag{6.1}$$

As already discussed in Chapter 5, the received signal passes the receiver MF and DMF. Regarding to [12], the mathematical context is given below. At both filters, the output signal samples can be expressed as follows:

$$y_0(t) = r'(t) \otimes h(t) = z_0(t) + n_0(t) \tag{6.2}$$

$$y_{0,k} = y_0(kT) = z_{0,k} + n_{0,k} \tag{6.3}$$

$$y_1(t) = r'(t) \otimes h_1(t) = z_1(t) + n_1(t) \tag{6.4}$$

$$y_{1,k} = y_1(kT) = z_{1,k} + n_{1,k} \tag{6.5}$$

where $n_{0,k}$ and $n_{1,k}$ are the noise parts, which are zero-mean non-white Gaussian variates and $z_{0,k}$ and $z_{1,k}$ are the signal parts.

At the output of the timing error detector (TED), the output signal is given by

$$e_k = \mathrm{Re}[y^*_{0,k} y_{1,k}] \tag{6.6}$$

The derivation of the detector gain K_e results in

$$K_e = \frac{2}{3}A^2 \tag{6.7}$$

To control larger drifts, this estimator is designed with a second order loop filter. The transfer function is given by

$$F_e(z) = A + \frac{B}{z-1} \tag{6.8}$$

Thus, the corresponding z-transfer function results in

$$H_e(z) = \frac{1}{1 + \frac{F_e(z)}{z-1}} \tag{6.9}$$

Under the assumption that the noise sample n_k represent the input of the loop, the transfer function is given by

$$H_n(z) = H_e(z) - 1 = -\frac{B + A(z-1)}{B + A(z-1) + (z-1)^2} \tag{6.10}$$

In practice, the filter coefficients A and B are related to the natural frequency ω_n and to the dumping factor ζ. The relationships are as follows:

$$A = aK_e = 2\zeta\omega_n T \tag{6.11}$$

$$B = bK_e = (\omega_n T)^2 \tag{6.12}$$

Frequently $\zeta = 1$ is assumed, thus the relation of filter coefficients is $A^2 = 4B$. The mathematical derivation of the equivalent noise bandwidths, normalized to the symbol period T yield into

$$B_\tau T = \int_0^{1/2} |H_n(e^{j2\pi\nu})|^2 d\nu = \frac{5}{8}\sqrt{B} = \frac{5}{8}\omega_n T \tag{6.13}$$

$$B_\eta T = \int_0^{1/2} |H_\eta(e^{j2\pi\nu})|^2 d\nu = \frac{1}{8}B^{3/2} = \frac{1}{8}(\omega_n T)^3 \tag{6.14}$$

where the transfer function for timing drifts is given with,

$$H_\eta(z) = \frac{B(z-1)}{B + A(z-1) + (z-1)^2} \tag{6.15}$$

6.2 Modified Cramer-Rao Lower Bound and Jitter Variance

Symbol Timing

The jitter variance for the symbol timing can be written after some straightforward algebra by

$$\sigma^2_{\tau-\mathrm{NDA}} = \frac{B_\tau T}{K_e^2} A^2 \mathbb{E}[|n_{1,n}|^2] = \frac{27 B_\tau T}{128 \alpha \gamma_s} \tag{6.16}$$

Regarding to [10] the MCRLB for FB scheme is given by

$$\mathrm{MCRLB} = \frac{B_\tau T}{-T^2 \ddot{g}(0) \gamma_s} \tag{6.17}$$

Symbol Period

The computation of the jitter variance for the symbol period results in

$$\sigma^2_{\eta-\mathrm{NDA}} = \frac{B_\eta T}{K_e^2} A^2 \mathbb{E}[|n_{1,n}|^2] = \frac{27 (B_\tau T)^3}{250 \alpha \gamma_s} \tag{6.18}$$

Note that in the open literature no Cramer-Rao lower bound for the symbol period estimation could be found.

Comparing the equation for the jitter variance for symbol timing (6.16) and period (6.18) shows that the variances are directly proportional to the equivalent noise bandwidths and indirectly proportional to the roll-off factor and the SNR. Furthermore, it is clear that $\sigma^2_{\eta-NDA} \sim (B_\tau T)^3$.

6.3 Simulation Results

For the simulations the following parameter settings are used:

- Data frame: QPSK or 16-APSK modulated PRN sequences
- Oversampling with $N_s = 2$
- Roll-off factor $\alpha = 0.05$ and $\alpha = 0.25$
- Normalized residual frequency error $\sqrt{\text{MCRLB}(\nu)}$
- AWGN and random carrier phase $\theta \in [-\pi, \pi)$

6.3.1 Normalized Jitter Variance

In order to produce results comparable to those achieved with the FF scheme in Chapter 5, the normalized loop bandwidth $B_\tau T = 1/(2\,L/2)$ is chosen. Figure 6.2 to Figure 6.7 show the jitter variances of the timing estimates for different loop bandwidths and roll-off factors. Comparing the figures, it is clear that nearly all simulation results are close to the ML-NDA bound over the whole SNR range, and all results do not end up into an error floor. Only for a higher normalized loop bandwidth value, which means for a short length value and a very small roll-off factor given by $\alpha = 0.05$, the performance degrades rapidly in the lower SNR range . This can be explained due to the fact that noise components are non-linearly amplified in case of short length and small α. Using a higher roll-off factor, the performance for a smaller length value is definitely better in the lower SNR range. Furthermore, it is obvious that for lower normalized loop bandwidth values, good results are achieved over the whole SNR range, regardless of the roll-off factor value.

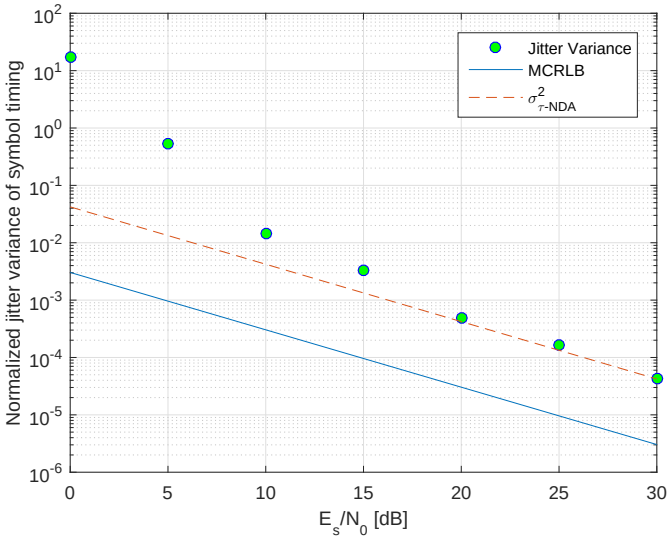

Figure 6.2: Normalized jitter variance for 16-APSK ($\alpha = 0.05, B_\tau T = 1 \times 10^{-2}$)

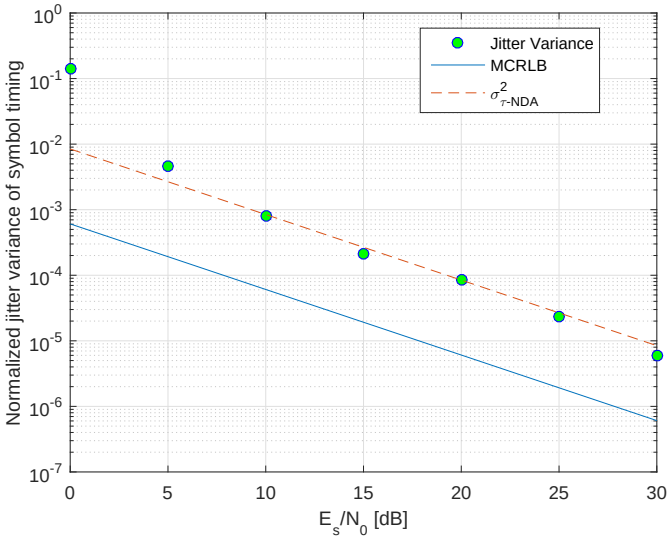

Figure 6.3: Normalized jitter variance for 16-APSK ($\alpha = 0.05, B_\tau T = 2 \times 10^{-3}$)

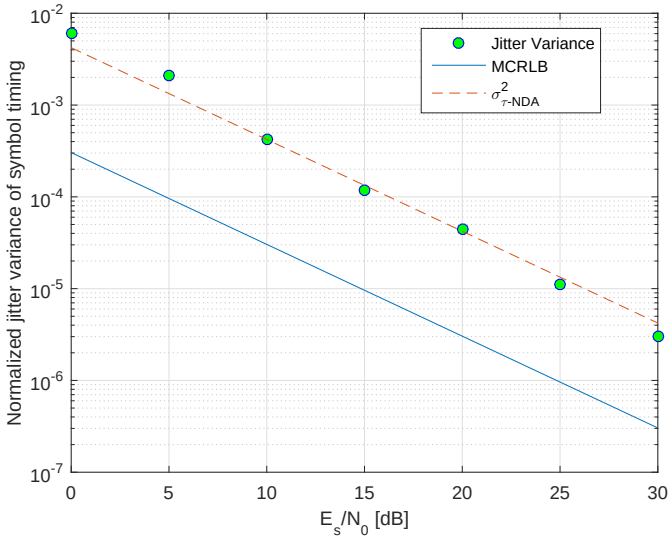

Figure 6.4: Normalized jitter variance for 16-APSK ($\alpha = 0.05, B_\tau T = 1 \times 10^{-3}$)

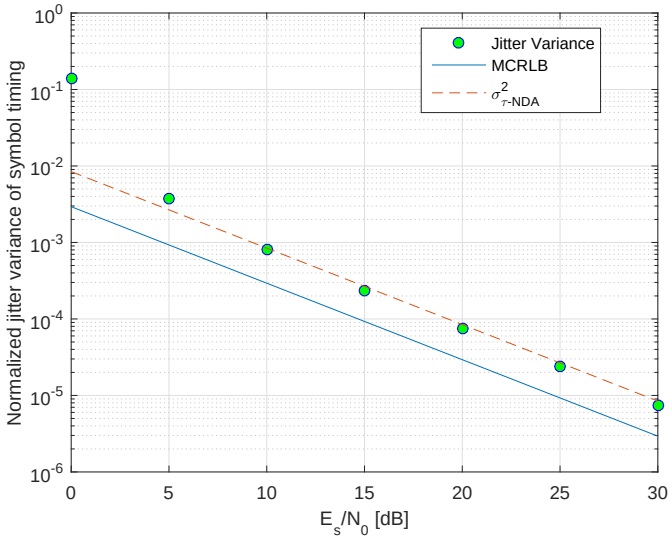

Figure 6.5: Normalized jitter variance for 16-APSK ($\alpha = 0.25, B_\tau T = 1 \times 10^{-2}$)

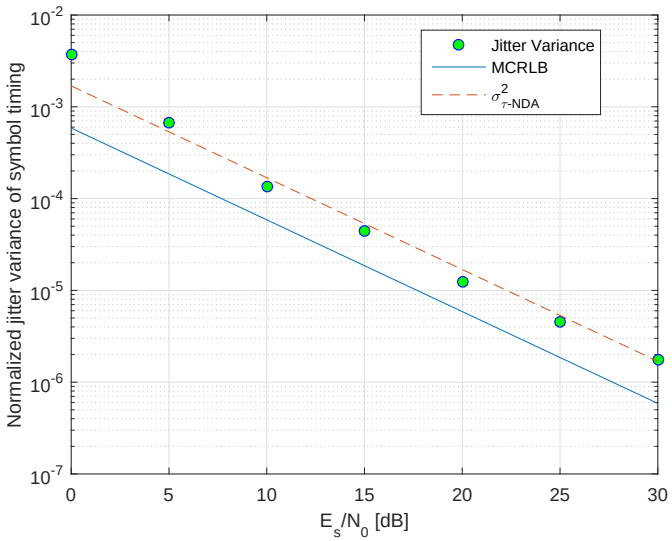

Figure 6.6: Normalized jitter variance for 16-APSK ($\alpha = 0.25, B_\tau T = 2 \times 10^{-3}$)

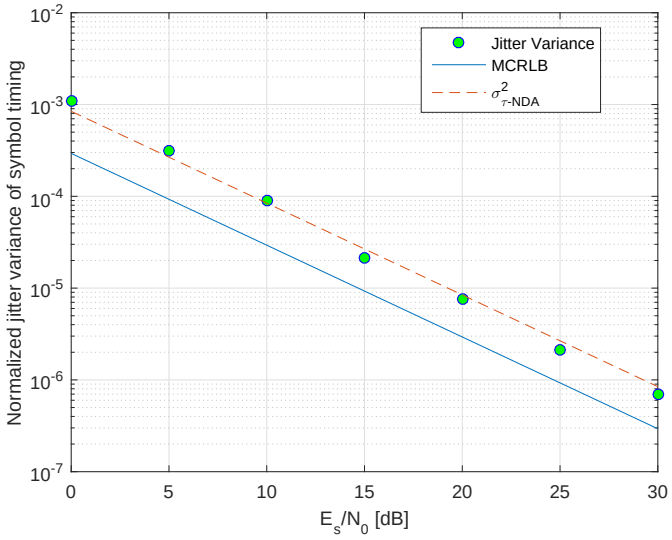

Figure 6.7: Normalized jitter variance for 16-APSK ($\alpha = 0.25, B_\tau T = 1 \times 10^{-3}$)

In Figures 6.8 to 6.11 the results of the symbol rate variance are depicted. It is obvious that nearly all variances are close to the ML-NDA bound over the whole SNR range. Also, it is visible that the results do not end up in a jitter floor. For a small roll-off factor, given by $\alpha = 0.05$, the results are illustrated in Figures 6.8 and 6.9, the results for higher α are depicted in Figures 6.10

and 6.11. Therefore, a similar behaviour as for the symbol timing estimates are observable. The results for QPSK modulated data do not differ from these results.

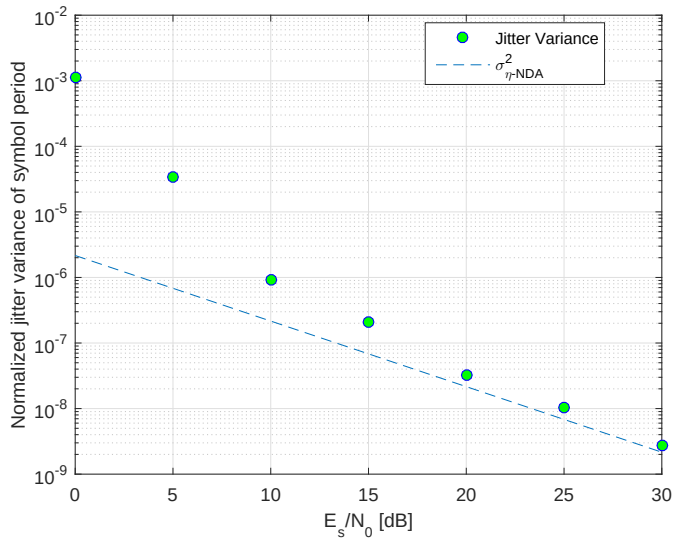

Figure 6.8: Normalized jitter variance for 16-APSK ($\alpha = 0.05, B_\tau T = 1 \times 10^{-2}$)

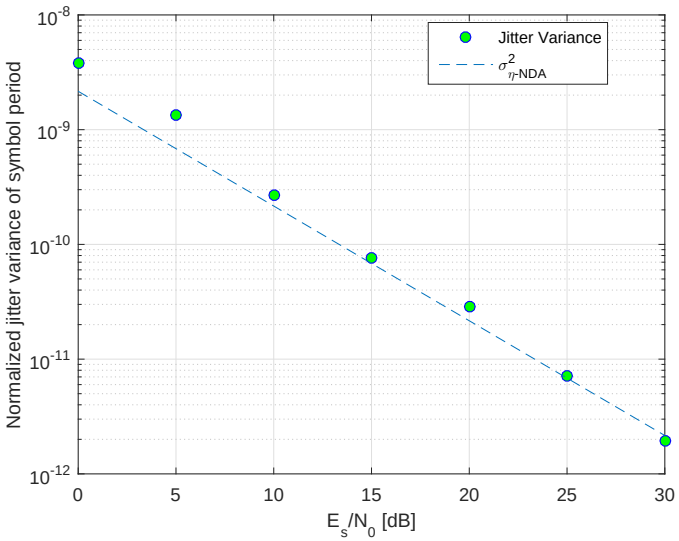

Figure 6.9: Normalized jitter variance for 16-APSK ($\alpha = 0.05, B_\tau T = 1 \times 10^{-3}$)

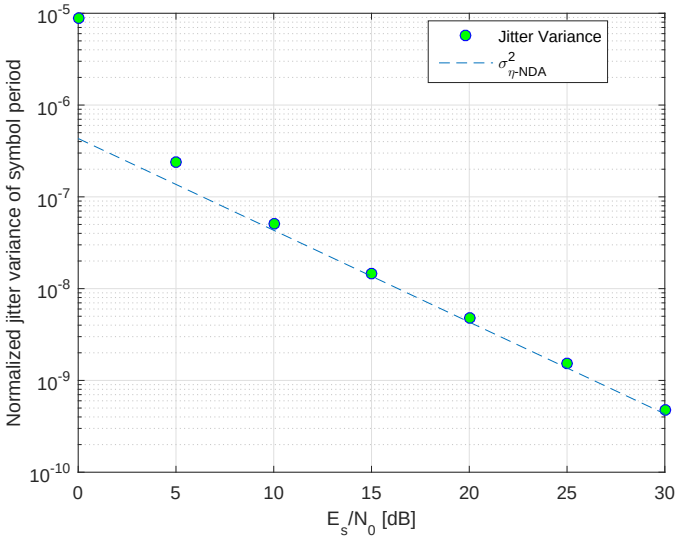

Figure 6.10: Normalized jitter variance for 16-APSK ($\alpha = 0.25, B_\tau T = 1 \times 10^{-2}$)

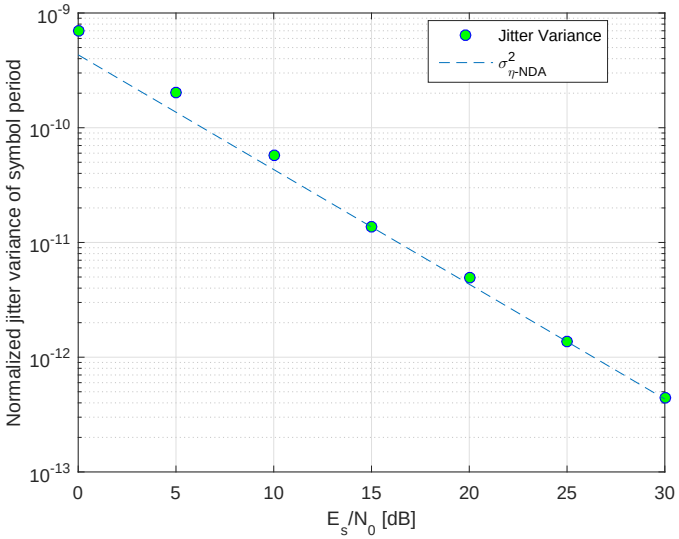

Figure 6.11: Normalized jitter variance for 16-APSK ($\alpha = 0.25, B_\tau T = 1 \times 10^{-3}$)

7 Conclusion

In this master thesis, four different symbol period, respectively symbol rate estimation methods have been investigated. Of course, all analysed algorithms have pros and cons, but all methods are capable to deliver reliable estimates for symbol timing and symbol rate. Inspecting the results of the joint data-aided parameter estimation, which uses a correlation filter bank, shows that if the spacing grid between the filter elements is too large or too small, the parabolic approach is not working successfully. In addition, it was observed that the suitable grid spacing depends on the pilot sequence length. It was interesting to see that these estimator results are independent from the roll-off factor. The analysis of the data-aided symbol rate estimation by timing shows that for very short preamble lengths the performance degrades in the lower SNR range. With longer preambles, better results could be achieved. Similar to the joint data-aided parameter estimation method, this algorithm is not affected by the roll-off factor.

The investigation of the hybrid DA/NDA algorithm, implemented via a FF scheme, provides a good estimation performance, but it has to be considered that the performance worsens with smaller roll-off factors due to the NDA estimator sensitivity. As well, at higher signal-to-noise ratios the jitter variance ends up in an error floor. It was also observed that the symbol timing estimates are better than the O&M estimates, but for the symbol period, both algorithms deliver similar results. The fourth method studied in the context of this thesis was a carrier-blind and non-data-aided tracking method implemented as FB scheme. Compared to the hybrid method, the jitter variances did not end up in a jitter floor at higher SNR values, but a dependency of the performance from the roll-off factor could be observed.

Bibliography

[1] U. Mengali and A. N. D'Andrea, *Synchronisation Techniques for Digital Receivers*. Plenum Press: New York, 1997.

[2] EN 302 307, "Digital Video Broadcasting (DVB); Second generation framing structure, channel coding and modulation systems for Broadcasting, Interactive Services, News Gathering and other broadband satellite applications; Part II: S2-Extensions (DVB-S2X)," *ETSI Standard*, 2014.

[3] M. Moeneclaey, "On the true and modified Cramer-Rao bounds for the estimation of a scalar parameter in the presence of nuisance parameters," *IEEE Trans.Commun.*, vol. 46, pp. 1536–1544, Nov. 1998.

[4] A. N. D'Andrea, U. Mengali, and R. Reggiannini, "The modified Cramer-Rao bound and its application to synchronization problems," *IEEE Trans. Commun.*, vol. 42, pp. 1391–1399, Feb./March/April 1994.

[5] W. Gappmair and A. Ginesi, "Cramer-Rao lower bound and parameter estimation for multibeam satellite links," *Int. J. Satell. Commun. Network.*, vol. 35, pp. 343–357, 2016.

[6] W. H. Press, S. A. Teukolsky, W. T. Vetterling, and B. P. Flannery, *Numerical Recipes in C: The Art of Scientific Computing. Second Edition*. Cambridge Univ. Press: New York, 1992.

[7] W. Gappmair, B. Suesser-Rechberger, and A. Ginesi, "Performance of Walsh-Hadamard Codes Used for Timing Recovery in a DVB-S2x Multibeam Scenario," *Proceedings of the 10^{th} International Symposium on Communication Systems, Networks and Digital Signal Processing (CSNDSP)*, Prague, Czech Republic, pp. 1-6, July 2016.

[8] R. Pedone, M. Villanti, A. Vanelli-Coralli, G. E. Corazza, and P. T. Mathiopoulos, "Frame synchronization in frequency uncertainty," *IEEE Trans. Commun.*, vol. 58, pp. 1235–1246, April 2010.

[9] M. Luise and R. Reggiannini, "Carrier frequency recovery in all-digital modems for burst-mode transmissions," *IEEE Trans. Commun.*, vol. 43, pp. 1169–1178, Feb./March/April 1995.

[10] W. Gappmair, S. Cioni, G. E. Corazza, and O. Koudelka, "Jitter floor elimination for blind feedforward/feedback symbol-timing recovery exploiting the extended zero-crossing property," *Int. J. Satell. Commun. Network.*, vol. 34, pp. 645–660, 2016.

[11] M. Oerder and H. Meyr, "Digital Filter and Square Timing Recovery," *IEEE Trans. Commun.*, vol. 36, pp. 605–612, May 1988.

[12] W. Gappmair, K. Plimon, and A. Ginesi, "Coarse recovery of carrier frequency and symbol timing in multibeam satellite channels," *Int. J. Satell. Commun. Network.*, Accepted for publication, 2017.